INL/RPT-23-74505

PARFUME/BISON Fission Product Release Predictions versus AGR-3/4 Heating Test Measurements

September 2023

William F. Skerjanc

Idaho National Laboratory

INL is a U.S. Department of Energy National Laboratory
operated by Battelle Energy Alliance, LLC

INL/RPT-23-74505

PARFUME/BISON Fission Product Release Predictions versus AGR-3/4 Heating Test Measurements

William F. Skerjanc

September 2023

Idaho National Laboratory
Advanced Reactor Technologies
Idaho Falls, Idaho 83415

http://www.art.inl.gov

Prepared for the
U.S. Department of Energy
Office of Nuclear Energy
Under DOE Idaho Operations Office
Contract DE-AC07-05ID14517

Page intentionally left blank

INL ART Program

PARFUME/BISON Fission Product Release Predictions versus AGR-3/4 Heating Test Measurements

INL/RPT-23-74505

September 2023

Technical Reviewer:

Adriaan Riet	9/12/2023
AGR PIE Analyst	Date

Approved by:

Paul A. Demkowicz	9/12/2023
AGR Fuels Technical Director	Date
Travis R. Mitchell	9/12/2023
ART Program Manager	Date
Michelle T. Sharp	9/12/2023
INL Quality Assurance	Date

ABSTRACT

The fuel performance modeling codes PARFUME (PARticle FUel ModEl) and BISON were used to predict the release of fission products silver, cesium, and strontium from fuel compacts containing tristructural isotropic (TRISO) coated particles during heating tests post irradiation. The AGR-3/4 fuel compacts were irradiated as part of the third and fourth series of planned experiments to support the Advanced Gas Reactor (AGR) program. The heating tests were conducted at temperatures between 1200°C and 1700°C to evaluate fission product release at elevated temperatures. The measured fission product release fractions from the heating tests were compared to modeling predictions calculated by PARFUME and BISON to evaluate how the codes compare to experimental results.

Comparisons between the experimental measured fission product release fractions from silver, cesium, and strontium indicate that both modeling codes overpredict the fission product release fractions which demonstrate that the diffusivities used in the codes are overestimated. This results in a conservative estimate predicted by the codes when evaluating the fission product release relative to experimental data as it pertains to silver, cesium, and strontium.

Page intentionally left blank

CONTENTS

ABSTRACT iv
ACRONYMS xi
1. INTRODUCTION 1
1.1 AGR Program 1
1.2 PARFUME 2
1.3 BISON 3
2. AGR-3/4 EXPERIMENT 5
2.1 Fuel Characteristics 5
2.2 AGR-3/4 Description 6
2.3 AGR-3/4 Irradiation 9
2.4 Heating Tests 10
3. MODELING 12
3.1 Input Parameters 12
3.2 Irradiation Conditions 13
3.3 Heating Test Conditions 15
3.4 Fission Product Transport 16
4. RESULTS 21
4.1 Failure Probability 21
4.2 Compact 3-2 1600/1700°C Heating Test 24
4.3 Compact 8-2 1400°C Heating Test 25
4.4 Compact 10-2 1200°C Heating Test 27
4.5 Compact 10-4 1400°C Heating Test 28
5. ANALYSIS AND DISCUSSION 31
5.1 Silver Release 31
5.2 Cesium Release 34
5.3 Strontium Release 37
5.4 Compacts 8-2 and 10-4 39
5.5 Compacts 8-2 and 10-2 41
6. CONCLUSION 44
7. REFERENCES 46

FIGURES

Figure 1. PARFUME calculation flow chart. 3
Figure 2. Monte Carlo methodology for calculating failure probability in BISON. 4
Figure 3. Typical TRISO-coated fuel particle geometry. 5
Figure 4. Schematic of an AGR-3/4 compact with DTF fuel particles along the axis. 6
Figure 5. ATR core cross section displaying the NEFT position. 7
Figure 6. Axial schematic of the AGR-3/4 capsules. 8
Figure 7. Radial schematic of the AGR-3/4 capsule. 8
Figure 8. Simplified flow path for the AGR-3/4 sweep gas. 9
Figure 9. Graphic of the FACS furnace used to conduct heating tests. 11
Figure 10. Evolution of daily temperatures and silver production throughout irradiation for Compact 10-2 and Compact 8-2. 15
Figure 11. Evolution of FACS furnace heating tests temperatures for selected as-irradiated AGR-3/4 compacts. 16
Figure 12. Silver diffusivities. 19
Figure 13. Cesium diffusivities. 19
Figure 14. Strontium diffusivities. 20
Figure 15. Driver fuel particle failure probability for selected AGR-3/4 compacts. 23
Figure 16. Compact 3-2 measured fission product release fraction versus PARFUME (PFM) and BISON (BSN) from the 1600/1700°C heating test. 24
Figure 17. End of the heating test measured release fractions (HT) versus the predicted release fractions for Compact 3-2. 25
Figure 18. Compact 8-2 measured fission product release fraction versus PARFUME (PFM) and BISON (BSN) from the 1400°C heating test. 26
Figure 19. End of the heating test measured release fractions (HT) versus the predicted release fractions for Compact 8-2. 27
Figure 20. Compact 10-2 measured fission product release fraction versus PARFUME (PFM) and BISON (BSN) from the 1200°C heating test. 27
Figure 21. End of the heating test measured release fractions (HT) versus the predicted release fractions for Compact 10-2. 28
Figure 22. Compact 10-4 measured fission product release fraction versus PARFUME (PFM) and BISON (BSN) from the 1400°C heating test. 29
Figure 23. End of the heating test measured release fractions (HT) versus the predicted release fractions for Compact 10-4. 30
Figure 24. Measured silver (Ag-110m) release fraction evolution versus PARFUME (PFM) and BISON (BSN). 32
Figure 25. End of the heating test measured silver (Ag-110m) release fractions (HT) versus the predicted release fractions. 32

Figure 26. Measured silver (Ag-110m) release fraction rate evolution versus PARFUME (PFM) and BISON (BSN). 34
Figure 27. Measured cesium (Cs-134) release fraction evolution versus PARFUME (PFM) and BISON (BSN). 35
Figure 28. End of the heating test measured cesium (Cs-134) release fractions (HT) versus the predicted release fractions. 35
Figure 29. Measured cesium (Cs-134) release fraction rate evolution versus PARFUME (PFM) and BISON (BSN). 36
Figure 30. Measured strontium (Sr-90) release fraction evolution versus PARFUME (PFM) and BISON (BSN). 37
Figure 31. End of the heating test measured strontium (Sr-90) release fractions (HT) versus the predicted release fractions. 38
Figure 32. Measured strontium (Sr-90) release fraction rate evolution versus PARFUME (PFM) and BISON (BSN). 39
Figure 33. Measured silver (Ag-110m) release fraction versus PARFUME (PFM) and BISON (BSN) for Compacts 8-2 and 10-4 at 1400°C. 40
Figure 34. Measured cesium (Cs-134) release fraction versus PARFUME (PFM) and BISON (BSN) for Compacts 8-2 and 10-4 at 1400°C. 41
Figure 35. Measured strontium (Sr-90) release fraction versus PARFUME (PFM) and BISON (BSN) for Compacts 8-2 and 10-4 at 1400°C. 41
Figure 36. Measured silver (Ag-110m) release fraction versus PARFUME (PFM) and BISON (BSN) for Compacts 8-2 and 10-2. 42
Figure 37. Measured cesium (Cs-134) release fraction versus PARFUME (PFM) and BISON (BSN) for Compacts 8-2 and 10-2. 43
Figure 38. Measured strontium (Sr-90) release fraction versus PARFUME (PFM) and BISON (BSN) for Compacts 8-2 and 10-2. 43

TABLES

Table 1. Primary functions of particle fuel components. 6
Table 2. Capsule average thermal conditions and end-of-irradiation fluence and burnup. 10
Table 3. FACS furnace condensation plate fission product collection efficiencies at 1600°C. 11
Table 4. Parameters used in PARFUME to model the AGR-3/4 irradiation test. 13
Table 5. Selected AGR-3/4 compacts end-of-irradiation TAVA temperatures, accumulated fluence and burnup, and heating test temperatures. 14
Table 6. Diffusion coefficients used in PARFUME and BISON. 17
Table 7. Driver fuel particle failure probability for selected AGR-3/4 compacts 23
Table 8. Pd penetration for selected AGR-3/4 compacts 23
Table 9. Measured and predicted release fractions at the end of Compact 3-2 heating test. 24

Table 10. Measured and predicted release fractions at the end of Compact 8-2 heating test. 26
Table 11. Measured and predicted release fractions at the end of Compact 10-2 heating test. 28
Table 12. Measured and predicted release fractions at the end of Compact 10-4 heating test. 29
Table 13. Measured and predicted silver (Ag-110m) release fractions at the end of the heating tests. 33
Table 14. Measured and predicted silver (Ag-110m) retention fraction at the end of the AGR-3/4 irradiation..... 33
Table 15. Measured and predicted cesium (Cs-134) release fractions at the end of the heating tests. 35
Table 16. Measured and predicted strontium (Sr-90) release fractions at the end of the heating tests. 38
Table 17. Irradiation conditions and heating test temperature for Compacts 8-2 and 10-4. 39
Table 18. Irradiation conditions and heating test temperature for Compacts 8-2 and 10-2. 42

Page intentionally left blank

ACRONYMS

AGR	Advanced Gas Reactor
ART	Advance Reactor Technologies
ATR	Advanced Test Reactor
BAF	Bacon anisotropy factor
CEGA	Combustion Engineering/General Atomics
DTF	designed-to-fail
EFPD	effective full power days
FACS	Fuel Accident Condition Simulator
FB	fuel body
FIMA	fissions per initial heavy metal atom
HTGR	high-temperature gas reactor
IAEA	International Atomic Energy Agency
INL	Idaho National Laboratory
IPyC	inner pyrolytic carbon
LEU	low-enriched uranium
MDA	minimum detectable activity
MOOSE	Multiphysics Object-Oriented Simulation Environment
NEFT	northeast flux trap
OPyC	outer pyrolytic carbon
PyC	pyrolytic carbon
PALM	power axial locator mechanism
PARFUME	PARticle FUel ModEl
PIE	post-irradiation examination
SiC	silicon carbide
TAVA	time-average/volume-average
TMAP4	Tritium Migration Analysis Program Version 4
TRISO	tristructural isotropic
UCO	uranium oxycarbide

Page intentionally left blank

PARFUME/BISON Fission Product Release Predictions versus the AGR-3/4 Safety Test

1. INTRODUCTION

Several fuel and material irradiation experiments have been completed during Idaho National Laboratory's (INL's) Advanced Reactor Technologies (ART) Advanced Gas Reactor (AGR) Fuel Development and Qualification Program. These experiments support the development and qualification of tristructural isotropic (TRISO)-coated particle fuel for use in high-temperature gas-cooled reactors (HTGRs). The goals of these experiments are to provide irradiation performance data to support fuel process development, qualify fuel for normal operating conditions, support the development and validation of fuel performance and fission product transport models and codes, and provide irradiated fuel and materials for post-irradiation examination (PIE) and safety testing (Mitchell and Demkowicz 2022). AGR-3/4 combined the third and fourth in this series of experiments to test TRISO-coated, low-enriched uranium (LEU) oxycarbide (UCO) fuel.

This report documents comparisons between the fission product release during heating tests of selected AGR-3/4 fuel compacts and the corresponding fission product release fractions predicted by the fuel performance modeling code PARticle FUel ModEl (PARFUME) (Miller, Petti, et al. 2023) and the finite element-based code BISON (Williamson, et al. 2021) for silver (Ag), cesium (Cs), and strontium (Sr). The calculations include modeling AGR-3/4 compacts irradiated from December 2011 to April 2014 in the Advanced Test Reactor (ATR) over a total of 10 ATR cycles, including seven normal cycles, one low-power cycle, one unplanned outage cycle, and one power axial locator mechanism (PALM) cycle for a total of 369.1 effective full power days (EFPD). Because no burnup was accumulated during the low-power cycle and the AGR-3/4 test train was moved to the ATR canal during the unplanned outage and PALM cycles, the modeling only covers the seven normal power cycles. Heating tests were then performed on selected as-irradiated fuel compacts using the Fuel Accident Condition Simulator (FACS) furnace at INL in a range of postulated reactor accident conditions (Stempien, et al. 2018) and the experimental fission product release fraction was compared to the predicted values from the fuel performance codes. Previous heating test comparisons were performed using PARFUME and PIE data from the AGR-1 (Collin 2014) and AGR-2 (Skerjanc 2020) experiments. In addition, the AGR-3/4 in-pile silver release predictions from PARFUME/BISON were performed and compared to PIE measurements along with the transport of silver, cesium, and strontium across selected AGR-3/4 capsule rings (Skerjanc and Jiang 2022).

Details associated with completing these calculations along with the experimental measurement data are provided in the remainder of this document. The AGR-3/4 irradiation experiment is described briefly in Section 2, PARFUME and BISON modeling input parameters are described in Section 3, compact modeling results are compared to the measured values from the heating tests in Section 4 and analysis of the results are discussed in Section 5, conclusions are summarized in Section 6, and the references are listed in Section 7.

1.1 AGR Program

The Department of Energy AGR Fuel Development and Qualification program was established to qualify TRISO-coated fuel for use in HTGRs. The primary goal of the program is to provide a baseline fuel qualification data set in support of the licensing and operation of an HTGR (Mitchell and Demkowicz 2022).

Seven fuel and material irradiation experiments were planned for the Department of Energy AGR program. The overall objectives of these experiments are to (Mitchell and Demkowicz 2022):

- Develop fuel fabrication capabilities
- Perform fuels and materials irradiation
- Perform safety testing and PIE
- Improve fuel performance modeling
- Evaluate fission product transport and source term determination.

1.2 PARFUME

INL developed the fuel performance code PARFUME (Miller, Petti, et al., PARFUME Theory and Model Basis Report 2023) to calculate the failure probability of a population of TRISO-coated fuel particles under irradiation and accident conditions. Calculations were performed with PARFUME Version 2.24 (as configured by the Revision Control System) and compiled with an Intel FORTRAN Compiler on a CentOS operating system. PARFUME was executed to calculate the particle failure probabilities and obtain the fractional releases of fission products using its fast integration and Monte Carlo solution schemes.

PARFUME is an integrated mechanistic computer code that evaluates the thermal, mechanical, and physicochemical behavior of coated fuel particles and the probability for fuel failure given the particle-to-particle statistical variations in physical dimensions and material properties that arise during the fuel fabrication process (Miller, Petti, et al. 2023). The objective in developing PARFUME is to physically describe the mechanical and physicochemical behavior of the fuel particle under irradiation and postulated accident conditions while capturing the statistical nature of the fuel behavior. The PARFUME code was developed to determine the failure probability of a population of fuel particles, accounting for viable mechanisms that can lead to particle failure. In addition, PARFUME calculates fission product transport by determining the diffusion of fission products from the LEU fuel kernel, through the particle coating layers, and their subsequent release through the compact/pebble matrix to the coolant boundary. The general solution procedure used by PARFUME consists of the basic processes depicted in the flow chart of Figure 1.

Coated particle fuel exhibits particle-to-particle variations in physical dimensions and material properties due to the nature of its fabrication process. Particle behavior is also inherently multidimensional, further complicating model development. The failure probability of a batch of fuel particles depends on statistical variations in the fuel design parameters and variation in the characteristic strengths of the coating layers. The calculation of fuel particle failures implemented in PARFUME samples the fuel properties from a Gaussian statistical distribution, and the layer strengths are sampled from a Weibull statistical distribution (Kovacs, Bongartz and Goodin 1985) (Martin 2002). PARFUME allows for statistical variations in the kernel diameter, layer thicknesses, pyrocarbon densities, degree of anisotropy of the pyrocarbons (as measured by the Bacon anisotropy factor [BAF]), the creep coefficient for the pyrocarbon, Poisson's ratio in creep for the pyrocarbon, bond strength between the inner pyrocarbon (IPyC) and SiC layers, and particle asphericity (as measured by the aspect ratio).

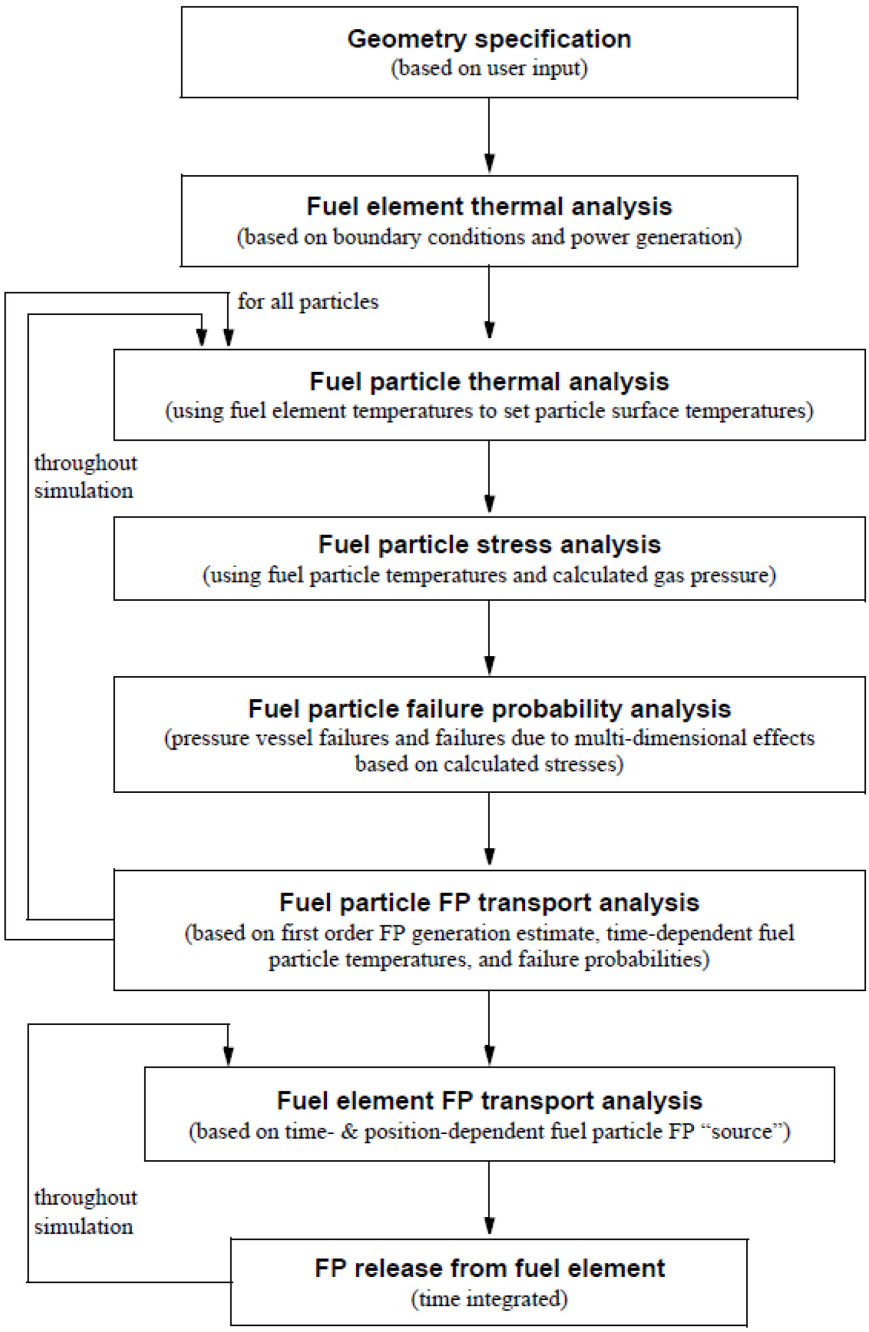

Figure 1. PARFUME calculation flow chart.

1.3 BISON

BISON (Williamson, et al. 2021) is a nuclear fuel performance application built using the Multiphysics Object-Oriented Simulation Environment (MOOSE) finite element library (Permann, et al. 2020) developed at INL that is capable of modeling multiple fuel forms in a wide variety of dimensions and geometries. BISON/MOOSE solves coupled nonlinear partial differential equations, including heat conduction, mechanics, fission product species transport, etc., in a fully implicit manner. More detailed descriptions of the BISON fuel performance code as it relates to TRISO fuel modeling can be found in

"BISON TRISO Modeling Advancements and Validation to AGR-1 Data" (Hales 2021), "Numerical Evaluation of AGR-2 Fission Product Release" (Hales, Toptan, et al. 2022), and "TRISO particle fuel performance and failure analysis with BISON" (Jiang, Hales, et al. 2021). The Monte Carlo methodology used in BISON to calculate the failure probability of a batch of fuel particles is summarized in Figure 2 (Jiang, Hales, et al. 2021). Recently, a more efficient statistical failure analysis, similar to the "fast" integration methodology in PARFUME, has been added to BISON (Jiang, Singh, et al. 2022).

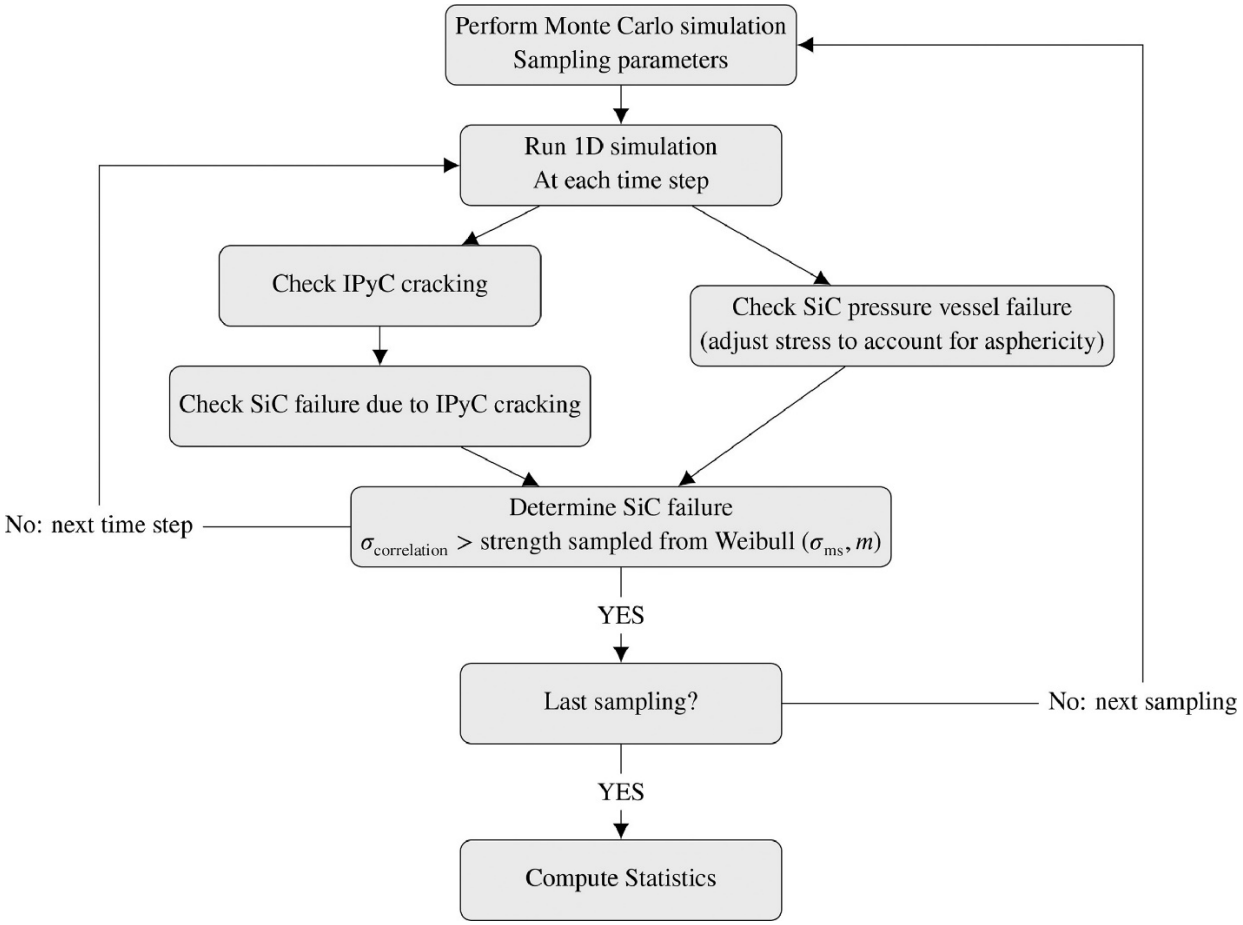

Figure 2. Monte Carlo methodology for calculating failure probability in BISON.

BISON has the capability to incorporate different irradiation conditions and run either very small analyses with a single processor or very large analyses on multiple processors on a supercomputer. For TRISO fuel, BISON supports spherically symmetric models, axisymmetric models, and full 3D models. Thermomechanical models for each material layer include elastic, irradiation creep, irradiation-induced dimension change, thermal expansion, and thermal conductivity.

Fission product generation, diffusion, and release can also be modeled for TRISO particles with UO_2, UCO, or uranium nitride kernels. In addition, BISON can perform statistical failure analyses of large samples of fuel particles, a capability that enables evaluation of failure due to multidimensional phenomena by analyzing thousands of particles. This enables realistic calculations of the fission product release from the many particles in a TRISO-fueled reactor.

2. AGR-3/4 EXPERIMENT

As defined in the technical program plan for the INL ART/AGR fuel program (Mitchell and Demkowicz 2022), the AGR-3/4 experiment objectives are:

1. Irradiate fuel containing UCO designed-to-fail (DTF) fuel particles that will provide a known source of fission products for subsequent transport through compact matrix and structural graphite materials
2. Assess the effects of sweep gas impurities (such as CO, H_2O, and H_2) typically found in the primary coolant circuit of HTGRs, on fuel performance and subsequent fission product transport
3. Provide irradiated fuel and material samples for PIE and post-irradiation heating tests
4. Support the refinement of fuel performance and fission product transport models with online, PIE, and post-irradiation heating test data.

2.1 Fuel Characteristics

Fuel for AGR-3/4 contained conventional driver fuel similar to the baseline fuel used in the AGR-1 experiment (Barnes 2006a) and DTF fuel particles whose kernels were identical to the driver fuel kernels with a single coating layer that was DTF under irradiation, leaving fission products to migrate through the surrounding materials (Barnes 2006b) (Marshall 2011).

- Driver fuel consisted of TRISO-coated particles that were slightly less than 1 mm in diameter. Each particle had a central reference kernel that contains fuel material, a porous carbon buffer layer, an IPyC layer, a SiC barrier coating, and an outer pyrolytic carbon (OPyC) layer as depicted in Figure 3. Each layer's function is described in Table 1. Kernels for AGR-3/4 consisted of only UCO fuel.
- DTF fuel consisted of reference kernels with a 20-µm-thick pyrolytic carbon (PyC) seal coating. This coating was DTF early in the irradiation and provide a known source of fission products.

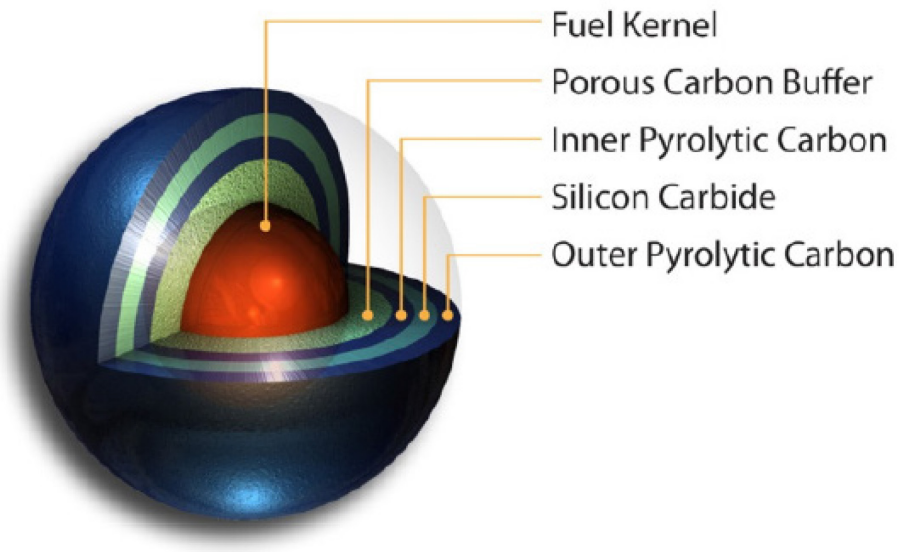

Figure 3. Typical TRISO-coated fuel particle geometry.

Table 1. Primary functions of particle fuel components.

Component	Primary Function
Kernel	Contains fissile fuel.
Buffer	Provides void space for fission product gases and accommodates differential changes in dimensions between coating layers and kernel.
IPyC	Structural layer and fission gas barrier that protects the kernel during SiC deposition and the SiC layer from most fission products during irradiation.
SiC	Primary structural layer and primary fission product barrier.
OPyC	Structural layer that also permits embedding the particles in graphitic matrix material.

Kernels for AGR-3/4 consisted of LEU UCO fuel. The kernels were fabricated by BWX Technologies (BWXT 2006) in accordance with the AGR-3/4 DTF Fuel and Capsule Component Material Specifications (Marshall 2011). The UCO kernels were coated and characterized by Oak Ridge National Laboratory (Hunn 2007) (Hunn 2011). Coating was performed in accordance with the AGR-3/4 fuel product specification (Barnes 2006b) (Marshall 2011).

After coating, AGR-3/4 fuel was formed into cylindrical compacts. The compact matrix material was composed of graphite flake and a thermosetting resin. Prior to compacting, the fuel particles were overcoated with thick layers of the compact matrix material. This overcoat was intended to prevent particle-to-particle contact and help achieve the desired packing fraction of the fuel particles. Each AGR-3/4 compact contained driver fuel particles and 20 DTF particles (making up about 1% of all the particles in each AGR-3/4 compact) that were placed along its center axis (Figure 4). AGR-3/4 compacts were nominally 12.51 mm in length and 12.31 mm in diameter. A complete description of the fuel compacts, fission product monitoring system, physics analysis, and thermal analysis were presented in the final as-run report (Collin 2016).

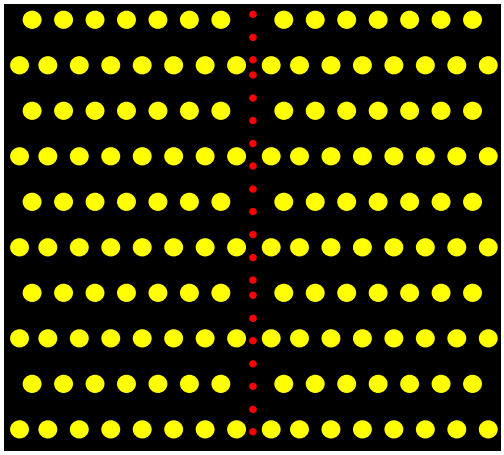

Figure 4. Schematic of an AGR-3/4 compact with DTF fuel particles along the axis.

2.2 AGR-3/4 Description

To achieve the test objectives outlined above in accordance with requirements from the technical program plan (Mitchell and Demkowicz 2022) and the irradiation test specification (Maki 2011), AGR-3/4 was irradiated in the northeast flux trap (NEFT) position of the ATR at INL. A cross-sectional view of the ATR core, which indicates the NEFT location, is displayed in Figure 5.

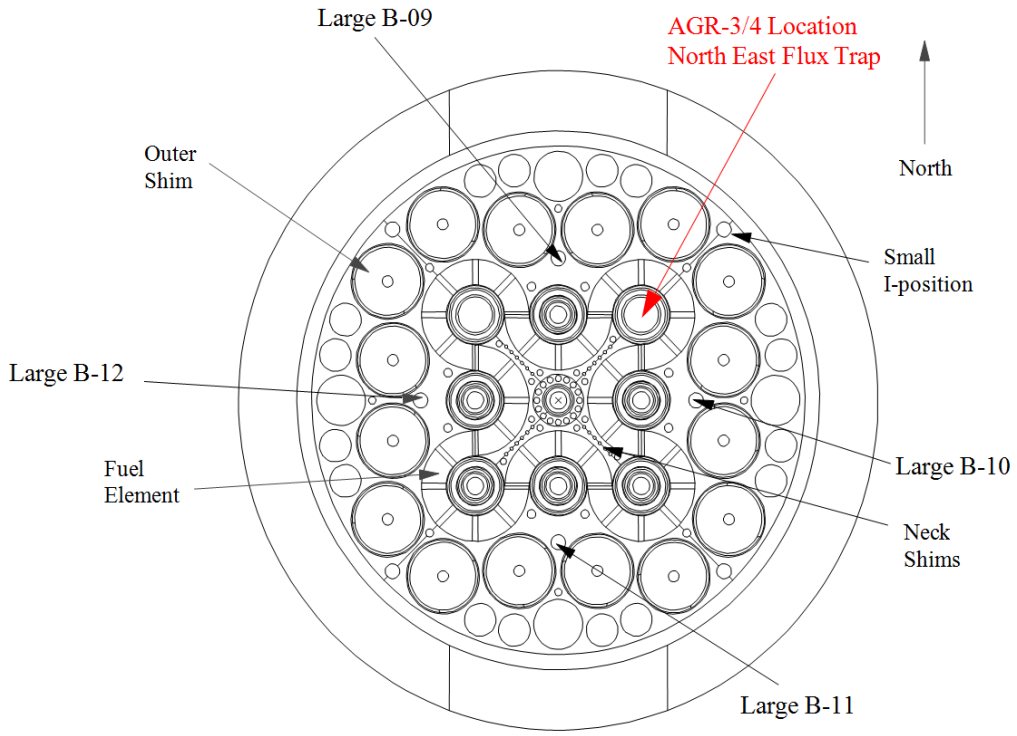

Figure 5. ATR core cross section displaying the NEFT position.

The AGR-3/4 test train was a multi-capsule, instrumented experiment designed for irradiation in the 133.4-mm-diameter NEFT position of ATR. The best geometry for obtaining radial fission product transport data was determined to be a capsule with a single stack of fuel compacts that contained a known fraction of DTF particles surrounded by three concentric annular rings of test material: an annulus of fuel-compact matrix material (in some capsules graphite was substituted for this ring); an annulus of fuel-element graphite; and an annulus of graphite operating at a lower temperature to act as a sink for fission products. This configuration was intended to reduce axial thermal gradients and, hence, axial diffusion. The test reactor's axial flux distribution and space considerations within the test train imposed a practical limit of 12 independently controlled and monitored capsules per test train. The capsules are stacked with Capsule 1 located at the bottom and Capsule 12 at the top. Similarly, the four compacts are stacked within each capsule with compact 1 at the bottom and compact 4 at the top. Hence, the compact naming convention begins with the capsule number followed by the compact number. For example, Compact 3-2 is located in Capsule 3 and is the second compact from the bottom. An axial view of the test train is illustrated in Figure 6. Figure 7 illustrates the radial view of a capsule.

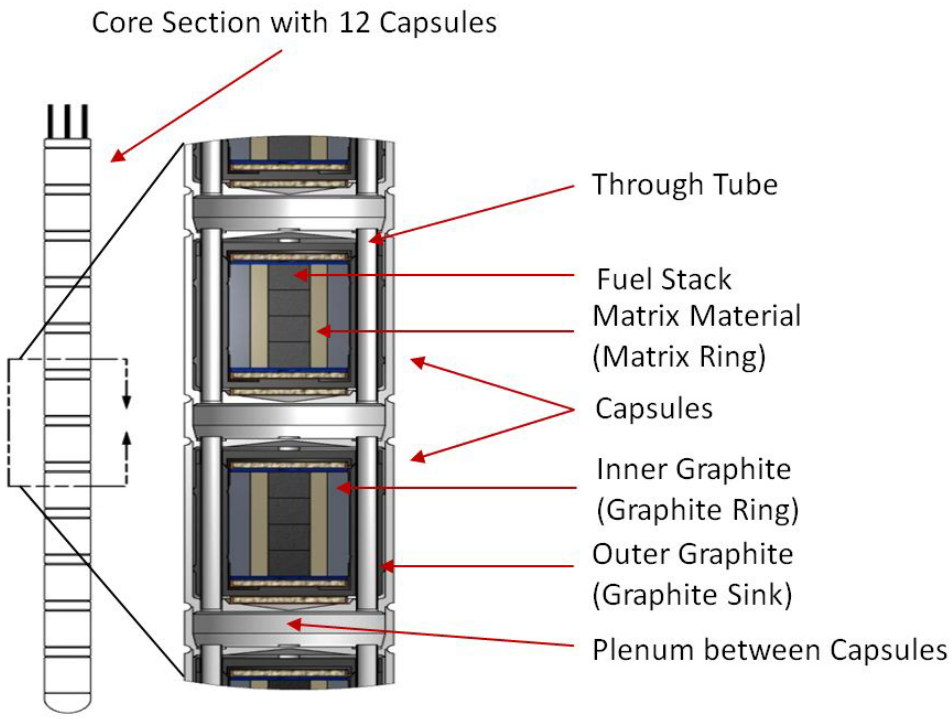

Figure 6. Axial schematic of the AGR-3/4 capsules.

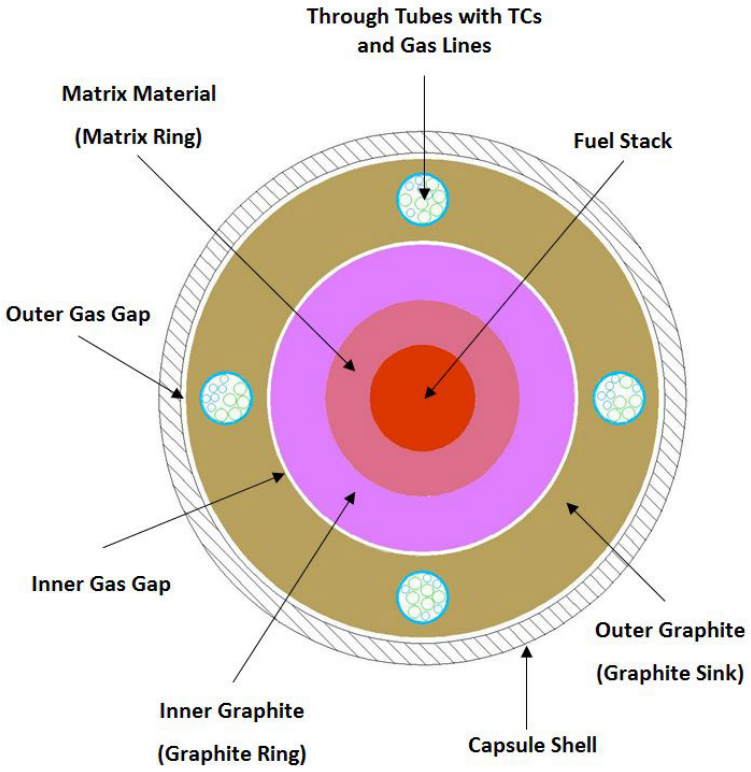

Figure 7. Radial schematic of the AGR-3/4 capsule.

Independent gas lines routed a mixture of helium and neon gases through each of the 12 capsules to provide temperature control and to sweep released fission product gases to the fission product monitoring system (Collin 2016). Figure 8 shows a schematic diagram of the fission product monitoring system.

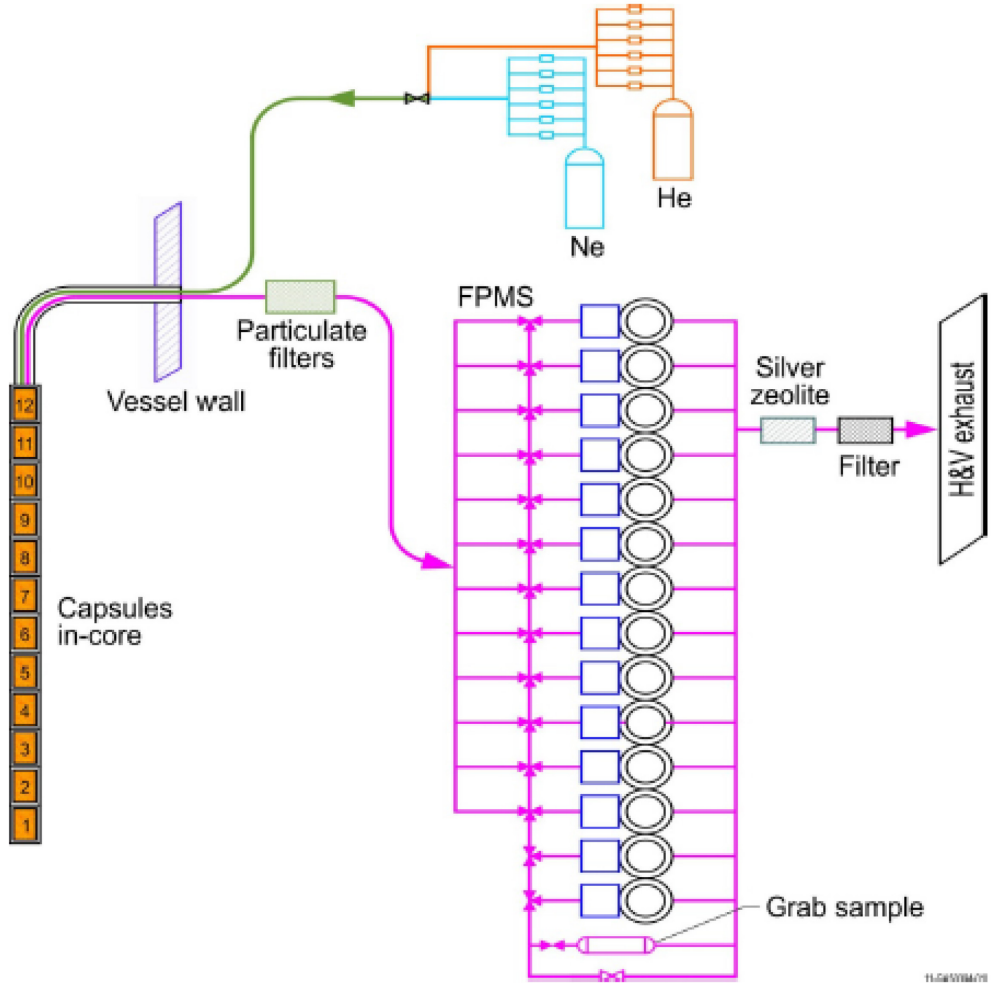

Figure 8. Simplified flow path for the AGR-3/4 sweep gas.

2.3 AGR-3/4 Irradiation

AGR-3/4 combined the third and fourth irradiation in the AGR program. Irradiation began in December 2011 and concluded in April 2014 in the ATR for a total irradiation duration of 369.1 EFPD. Final burnup values on a per compact basis ranged from 5.35 to 15.24% FIMA, while fast fluence values ranged from 1.50 to 5.31 × 10^{25} n/m^2 (E_n > 0.18 MeV). Time-average volume-averaged (TAVA) fuel temperatures on a capsule basis at the end of irradiation ranged from 854°C in Capsule 12 to 1345°C in Capsule 7. The capsule-specific fluence, burnup, and TAVA temperatures used for this study are shown in Table 2 (Collin 2016).

Table 2. Capsule average thermal conditions and end-of-irradiation fluence and burnup.

Capsule	Fluence ($\times 10^{25}$ n/m^2) [E_n > 0.18 MeV]	Burnup (% FIMA)	TAVA (°C)
12	1.50	5.35	854
11	2.87	9.06	1226
10	3.94	11.81	1191
9	4.66	13.67	1008
8	5.08	14.52	1190
7	5.27	14.96	1345
6	5.31	15.24	1051
5	5.19	14.88	1015
4	4.85	14.21	1008
3	4.22	12.58	1177
2	3.21	10.07	1057
1	1.76	6.14	927

2.4 Heating Tests

After irradiation, the AGR-3/4 test train was transferred to the Materials and Fuels Complex Hot Fuel and Examination Facility at INL, and PIE activities were divided into two phases (Demkowicz, AGR-3/4 Phase 2 Post-Irradiation Examination Plan 2017). The objectives of the AGR-3/4 PIE campaign are to (Demkowicz, AGR-3/4 Phase 2 Post-Irradiation Examination Plan 2017):

- Determine the distribution of fission products in matrix and graphite rings at the end of irradiation.
- Determine the distribution of fission products in matrix and graphite rings at elevated temperatures following heating in pure helium and/or oxidizing atmospheres.
- Determine the fractional inventory of the fission products remaining in fuel kernels and the compact matrix at the end of irradiation.
- Determine the fractional inventory of condensable and gaseous fission products released from fuel kernels and the compact matrix at elevated temperatures during heating in pure helium and/or oxidizing atmospheres.

Comparisons between experimental heating test fission product measurements and model predictions focused on silver, cesium, and strontium. The FACS furnace (Figure 9) at INL (Demkowicz, Laug, et al. 2012) was used to heat the selected as-irradiated compacts separately at a specified temperature. Helium sweep gas passed through the system at a flow rate of 1 L/min and the condensable fission products were collected on a condensation plate held on the end of a cold finger (Stempien, et al. 2018). These plates were exchanged throughout the tests and then gamma counted and examined for Sr-90 upon removal from the furnace. Dozens of plates may have been exchanged at prescribed time intervals during each test. The radionuclide inventories on each plate require correction by “collection efficiencies” for each element to estimate the true inventory that was released from the fuel. The efficiencies are defined as the inventory of a given element collected on the plate divided by the total inventory released from the fuel. The collection efficiencies are intended to account for the inventory that was lost to other areas inside the furnace besides the condensation plates. In applying a single collection efficiency for each element, the

assumption is that the collection efficiency is constant throughout the test. Furthermore, the FACS furnace currently has just one set of efficiencies that were experimentally determined at 1600°C. A campaign to measure collection efficiencies at other temperatures was conducted, and the data are under review. Additional collection efficiencies for temperatures other than 1600°C could be applied if and when they become available from that work.

The activities from the collected fission products were decay-corrected to the end of the AGR-3/4 irradiation plus one day. Further, the decay-corrected activities were then divided by the pre-determined FACS furnace condensation plate collection efficiencies summarized in Table 3 (Stempien, et al. 2018) (Demkowicz, Laug, et al. 2012) (Demkowicz, Reber, et al. 2015). To determine the compact release fraction (the ratio of measured inventory from the heating test to the total inventory in the compact produced during irradiation), the decay- and efficiency-corrected measured activities were divided by the predicted compact inventory from the AGR-3/4 physics calculations (Sterbentz 2015).

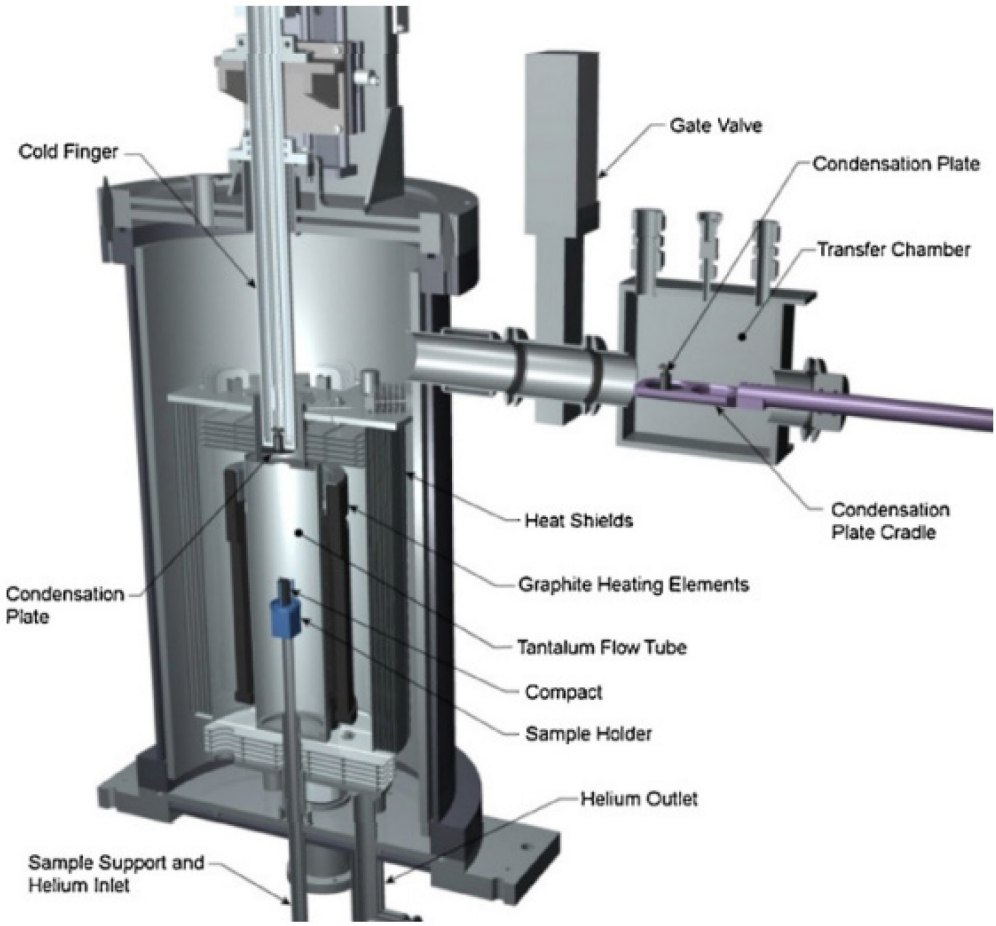

Figure 9. Graphic of the FACS furnace used to conduct heating tests.

Table 3. FACS furnace condensation plate fission product collection efficiencies at 1600°C.

Fission Product	1600°C Collection Efficiency
Ag	0.503
Cs	0.661
Sr	0.333

3. MODELING

PARFUME and BISON were used to model the AGR-3/4 experiment to determine the probability of fuel particle failure and release of the fission products silver, cesium, and strontium from both the driver fuel and DTF fuel particles. The analysis considered conventional fuel particle failure (e.g., typical pressure vessel failure) and multidimensional failure mechanisms (e.g., IPyC cracking, and pressure vessel failure associated with particle asphericity). The two fuel performance codes did not consider any as-fabricated exposed kernels and the release fractions were calculated assuming no driver fuel particle failures at time equal to zero. Both PARFUME and BISON assume that the DTF particles fail at the beginning of the irradiation. Key aspects of the modeling of the AGR-3/4 irradiation and heating tests are described in the following subsections.

3.1 Input Parameters

The PARFUME input parameters needed to model the AGR-3/4 irradiation experiment are provided in Table 4. They originate from:

- The "AGR-3/4 Irradiation Test Final As-Run Report" (Collin 2016) for the fuel characteristics, particle geometry, compact characteristics, and material non-mechanical properties.
- A Combustion Engineering/General Atomics (CEGA) Corporation report for the material mechanical properties (CEGA 1993).

In addition, diffusion coefficients used for fission product transport are derived from the International Atomic Energy Agency (IAEA) Technical Document 978 (IAEA 1997) and are discussed further below.

Table 4 displays parameters used in PARFUME. Material properties directly incorporated into the PARFUME source code have been previously discussed in detail (Miller, Petti, et al. 2018) (Miller and Knudson 2007) (Skerjanc and Collin 2018). Statistical variations are considered relative to the fuel attributes listed in Table 4 where the standard deviation is provided. This includes particle geometry, PyC densities, and PyC BAF.

Table 4. Parameters used in PARFUME to model the AGR-3/4 irradiation test.

Category	Parameter	Value
Fuel characteristics	U^{235} enrichment (wt%)	19.717
	Oxygen/uranium (atomic ratio)	1.43
	Carbon/uranium (atomic ratio)	0.361
Particle geometry	Kernel diameter (μm)	357.3 ± 10.5
	Buffer thickness (μm)	109.7 ± 7.7
	IPyC thickness (μm)	40.4 ± 2.3
	SiC thickness (μm)	33.5 ± 1.1
	OPyC thickness (μm)	41.3 ± 2.1
	Particle asphericity @ SiC (aspect ratio)	1.056
Compact characteristics	Diameter (mm)	12.31
	Number of driver particles per compact	1872
	Number of DTF particles per compact	20
	Compact matrix density (g/cm^3)	1.603
	Uranium contamination fraction	3.5×10^{-5}
Material properties	IPyC Weibull modulus	9.5
	SiC Weibull modulus	6
	OPyC Weibull modulus	9.5
	IPyC / SiC bond strength (MPa)	100
	PyC Poisson's ratio in creep	0.5
	PyC creep coefficient amplifier	2
	Kernel density (g/cm^3)	11.098
	Buffer density (g/cm^3)	1.10
	IPyC density (g/cm^3)	1.904 ± 0.014
	OPyC density (g/cm^3)	1.900 ± 0.012
	IPyC (post compact anneal) BAF	1.027 ± 0.002
	OPyC (post compact anneal) BAF	1.021 ± 0.002
DTF property	Pyrocarbon thickness (μm)	20.0 ± 0.9
	pyrocarbon density (g/cm^3)	1.988 ± 0.009
	Anisotropy	1.243 ± 0.019

3.2 Irradiation Conditions

PARFUME and BISON are designed to evaluate fuel performance based on user inputs for neutron fluence and burnup, with a corresponding set of thermal conditions. For this analysis, compact-specific fluence and burnup results from neutronics analysis (Sterbentz 2015) and fuel temperature histories from thermal analysis (Hawkes 2016) that were performed to support the AGR-3/4 experiment campaign were used in the models. The AGR-3/4 irradiation consisted of 48 compacts (Collin 2016) and the as-run model predictions were performed on a compact-level basis using their daily TAVA temperatures. The fluence, burnup, and final TAVA temperatures for the selected compacts are provided in Table 5 (Collin 2016).

Table 5. Selected AGR-3/4 compacts end-of-irradiation TAVA temperatures, accumulated fluence and burnup, and heating test temperatures.

Compact	Fluence (10^{25} n/m^2)	Burnup (%FIMA)	TAVA Irradiation Temperature (°C)	Heating Test Temperature (°C)
3-2	4.17	12.49	1196	1600/1700
8-2	5.11	14.58	1213	1400
10-2	4.01	11.96	1213	1200
10-4	3.75	11.43	1168	1400

PARFUME and BISON have considerable flexibility relative to the application of thermal conditions affecting fuel particles. A user may define the thermal conditions for the outer surfaces of the fuel-bearing materials (e.g., the outer surface of a pebble in the case of a pebble bed reactor or the coolant channel surface of a unit cell containing fuel compacts in the case of a prismatic reactor), or the user may define fuel-bearing material temperatures directly. Options for the outer surfaces of fuel-bearing materials include defining either a time-dependent set of temperatures or a time-dependent set of heat transfer coefficients, with a corresponding time-dependent set of sink temperatures. Fuel-bearing material temperatures can be defined directly as time-dependent values that are applicable to the entire material or the user may divide the material into regions and supply time-dependent temperatures for each region. The direct specification of fuel-bearing material temperatures was applied here at the outer surface of the OPyC layer using the predicted irradiation temperatures (Hawkes 2016).

The fuel performance predictive models assume all particles in a compact experience similar irradiation and thermal histories over the course of irradiation. Practically, they model one particle using the average burnup and fast neutron fluence and the volume-averaged temperature of the whole compact. In this scheme, PARFUME and BISON statistically treat a collection of particles within a range of geometrical dimensions and physical properties, but all the particles experience the same irradiation and thermal histories.

The AGR-3/4 experiment was irradiated for 369.1 EFPD and is modeled for each as-irradiated compact with end-of-irradiation values of burnup and fast neutron fluence summarized in Table 5. Burnup and fast neutron fluence are assumed to evolve linearly during irradiation. This assumption is validated by the nearly linear increase of the compact burnup and fast neutron fluence values reached at the end of each AGR-3/4 cycle, as reported in the AGR-3/4 as-run report (Collin 2016).

The thermal history evolves daily. For each compact, the daily temperatures of all the calculation nodes in a compact are averaged, and PARFUME and BISON use the resulting volume-averaged compact daily temperatures to set the thermal history of the modeled driver TRISO and DTF fuel particles. The daily temperatures are set as boundary conditions at the outer edge of the OPyC. From the OPyC boundary temperature, the codes calculate the temperature profile between the OPyC and the kernel center, considering that the temperature profile is affected throughout irradiation by the width of the gap forming between the buffer and the IPyC layer.

Daily temperatures were used in modeling because the TAVA temperatures (displayed in Table 5) were determined to not be a suitable metric to correlate fission product release to temperature, as they do not adequately reflect the thermal state of the compacts throughout irradiation. The compacts experienced a range of daily volume-average temperatures that could span several hundred degrees around their TAVA temperatures, resulting in a broad range of diffusivities, some of which far exceeded the diffusivity values calculated at the TAVA temperatures. The diffusivities are modeled with an Arrhenius equation and exponentially decrease with inverse temperatures. Consequently, diffusivity is highly sensitive to temperature, and averaging higher and lower temperatures with similar weights to compute

fission product release with the resulting TAVA temperature leads to an underestimation of the diffusivity, and hence an underestimation of the release.

As an illustration, Figure 10 shows the thermal histories of Compacts 10-2 and 8-2. Both compacts have a TAVA temperature of 1213°C, but Compact 8-2 experienced the highest temperatures over the last ~90 days of irradiation. Compact 8-2 is therefore expected to yield a higher fractional release of fission products. In this example, the silver release fraction calculated with the final TAVA temperature is 25% for both compacts. Using their respective daily temperatures, release fractions of 34% for Compact 10-2 and 56% for Compact 8-2 are obtained in accordance with the Arrhenius diffusivities. When comparing to the experimental measurements, using the daily temperatures to calculate release fractions is a much better metric to account for the effect of temperature on fission product release.

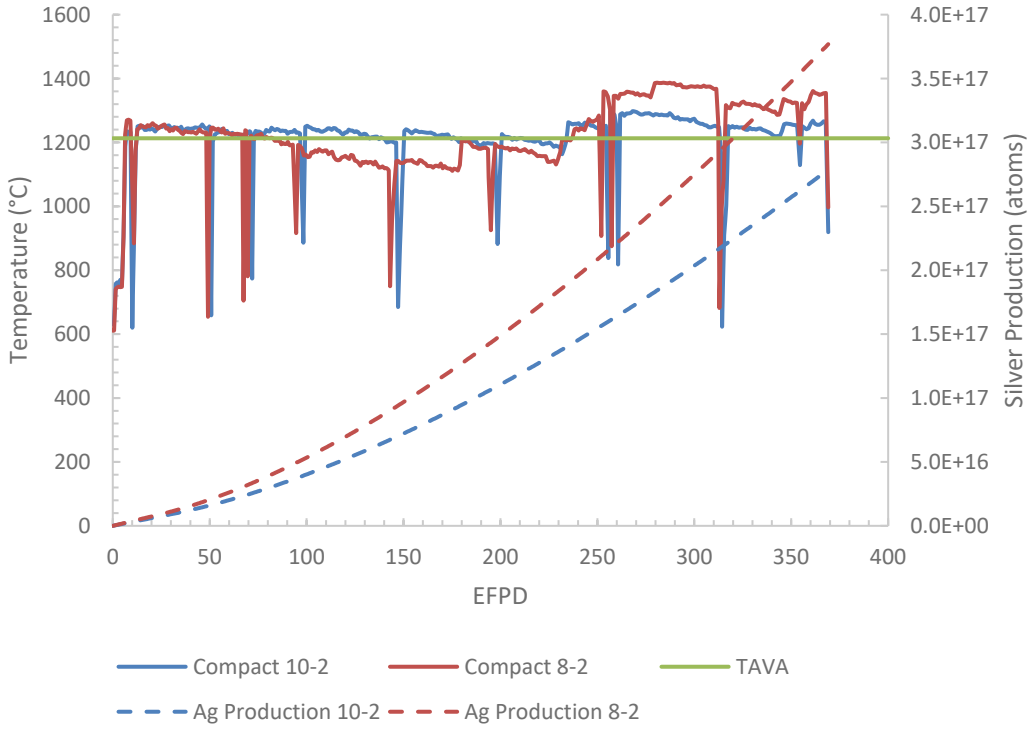

Figure 10. Evolution of daily temperatures and silver production throughout irradiation for Compact 10-2 and Compact 8-2.

3.3 Heating Test Conditions

With the exception of Compact 8-2, the other three compacts were selected based on their similar irradiation characteristics (see Table 5). The heating test evolution for these three compacts are described in "Preliminary results from the first round of post irradiation heating tests of fuel compacts from the AGR 3/4 irradiation" (Stempien, et al. 2018). Although not formally documented at the time of this publication, the heating test evolution for Compact 8-2 was similar to Compact 10-4. In general, the compacts were heated to approximately 300°C from ambient and held there for approximately two hours. Compacts 8-2, 10-2, and 10-4 were then heated to their planned isothermal hold temperatures (see Table 5) for approximately 300 hours while Compact 3-2 was heated to 1600°C for 330 hours and then to 1700°C for 50 hours. A summary of the heating test evolution for each compact is illustrated in Figure 11.

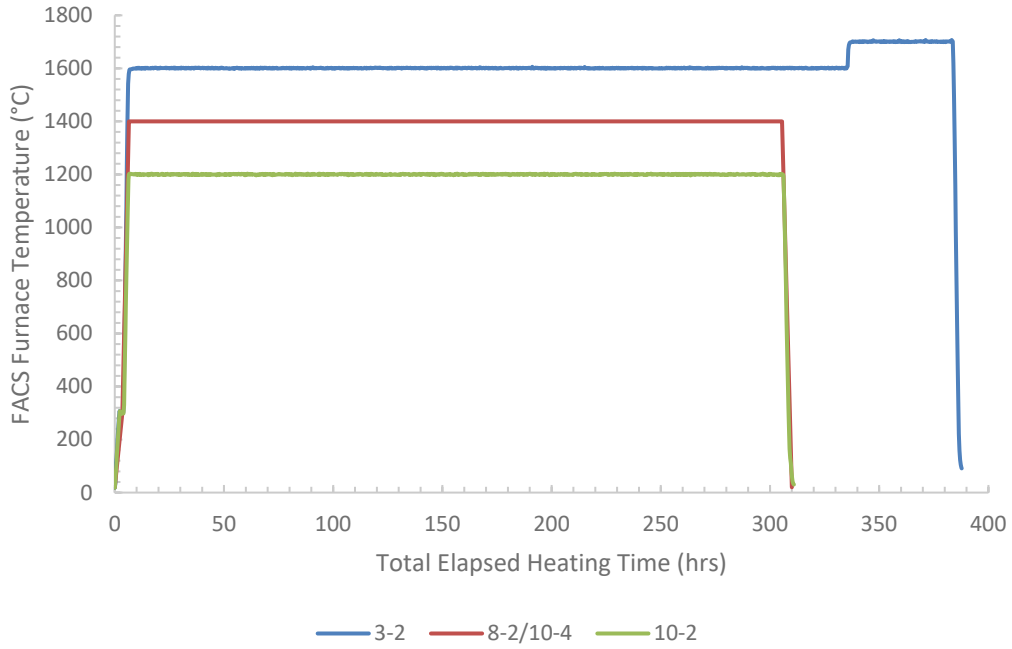

Figure 11. Evolution of FACS furnace heating tests temperatures for selected as-irradiated AGR-3/4 compacts.

3.4 Fission Product Transport

Fission product transport in PARFUME is based on coding extracted from the Tritium Migration Analysis Program Version 4 (TMAP4) (Longhurst, et al. 1992). Originally developed to assist in the evaluation of tritium losses from fusion reactor systems, TMAP4 incorporates a one-dimensional diffusion capability that determines the thermal response of structures and solves equations for solute atom movement through surfaces and in bulk materials.

The coding extracted from TMAP4 was modified for use within PARFUME to calculate fission product transport from the kernel through the successive coating layers of a TRISO-coated fuel particle, from individual TRISO-coated particles to the surrounding matrix, and from the surrounding matrix to the outside of the fuel sphere or compact, which constitutes the release of the fission products.

Fission product transport in PARFUME is a three-step process that includes a fuel element (e.g., cylindrical fuel compact comprised of many TRISO particles embedded in a graphitic matrix) thermal analysis, thermal and fission product transport analysis for fuel particles, and a fuel element fission product transport analysis ultimately leading to fission product release. Thermal analyses are performed to incorporate the temperature dependence of diffusion. Diffusion is first calculated for individual fuel particles. Results from each particle then serve as time- and position-dependent fission product sources for the subsequent fuel element transport analysis.

Fission product transport was calculated for silver, cesium, and strontium. Diffusion coefficients used in PARFUME and BISON for each of these species in the successive coating layers and matrix are derived from IAEA (IAEA 1997) and displayed in Table 6. The corresponding diffusivities can be calculated using these diffusion coefficients in the following Arrhenius-type equation:

$$D = D_{0,1}e^{-\frac{Q_{0,1}}{RT}} + D_{0,2}e^{-\frac{Q_{0,1}}{RT}}$$

where:

$D_{0,i}$ = pre-exponential factor (m^2/s)

$Q_{0,i}$ = activation energy (kJ/mol)

R = gas constant (8.3142×10^{-3} kJ/mol/K)

T = temperature (K)

The diffusion coefficients in Table 6 have been derived from the evaluation of numerous irradiation and heating experiments. They are defined as "effective" diffusion coefficients, "effective" meaning that all possible transport mechanisms are summarized in a single transport process. The use of these effective diffusion coefficients is to be considered with care. These coefficients were determined for UO_2 fuel and associated particle coatings of older German fabrication, whose properties (such as microstructure) are different than those of the UCO fuel and coatings of the AGR-3/4 experiment. Similar measurements for UCO fuel kernels (which can vary in stoichiometry) do not exist. Furthermore, in many cases, the coefficients employed here are partly based on data from post-irradiation heating tests and are conducted at higher temperatures than usual irradiation experiments. Consequently, IAEA diffusivities are not necessarily well adapted to model the fission product transport of the AGR-3/4 UCO fuel irradiation experiment.

Table 6. Diffusion coefficients used in PARFUME and BISON.

Specie	$D_{0,i}$ (m^2/s) $Q_{0,i}$ (kJ/mol)	Kernel[a]	Buffer	IPyC/OPyC	SiC	Matrix Graphite[b]
Ag	$D_{0,1}$	6.70E-09	1.00E-08	5.30E-09	3.60E-09	1.6
	$Q_{0,1}$	165	0	154	215	258
	$D_{0,2}$	--	--	--	--	--
	$Q_{0,2}$					
Cs	$D_{0,1}$	5.60E-08	1.00E-08	6.30E-08	5.50E-14	3.60E-04
	$Q_{0,1}$	209	0	222	125	189
	$D_{0,2}$	5.20E-04	--	--	1.60E-02	--
	$Q_{0,2}$	362			514	
Sr	$D_{0,1}$	2.20E-03	1.00E-08	2.30E-06	1.20E-09	1.00E-02
	$Q_{0,1}$	488	--	197	205	303
	$D_{0,2}$	--	--	--	1.80E+06	--
	$Q_{0,2}$				791	

a. Diffusivities used for UCO kernels were obtained from UO_2 data.

b. Diffusivity in the matrix was set to 10^{-6} m^2/s in cases where the release at the particle level was needed for comparison to experimental data.

The diffusivities of silver, cesium, and strontium as a function of temperature in the successive layers of a particle and compact are provided in the figures below. From these figures, the following conclusions can be drawn:

- Silver (Figure 12): SiC is the main retentive barrier, but the kernel and PyC are also slightly retentive. Considering the dimensions of the TRISO particle, the diffusion time through the kernel is not negligible compared to the diffusion time through the SiC layer. However, at the AGR-3/4 temperatures, these diffusion times are small compared to the irradiation length, and silver is not predicted to be well retained over the course of irradiation.

- Cesium (Figure 13): As with silver, the SiC layer is the main retentive barrier, but to a much larger extent than the kernel. The cesium diffusivity in SiC is about two-orders of magnitude lower than for silver in SiC. The kernel is also more retentive to cesium than it is to silver, which is an important factor in the case of particles with failed SiC layers. Because of its lower diffusivities, cesium is better retained than silver in both the kernel and SiC layer.
- Strontium (Figure 14): Unlike cesium and silver, strontium is primarily retained by the kernel itself. The combination of a larger thickness and a lower diffusivity compared to the SiC layer makes the kernel the first barrier to strontium release. Therefore, strontium release is less affected by the failure of the SiC layer than cesium, for example, and because of its low kernel diffusivity, strontium is well retained by the TRISO fuel at the AGR-3/4 temperatures.

The release of fission products is calculated at the compact level after the fission products were transported through the TRISO particle and surrounding compact. Fission products are considered released once they reach the compact edge. The fractional release of fission products is then calculated by normalizing the calculated release from the compact to the calculated kernel source or inventory.

To assess the release at the particle level, (i.e., the fission products that are released from the TRISO particle into the compact matrix), PARFUME and BISON can be modified to force diffusion through the matrix. This is done by adjusting the diffusivity of the graphitic matrix to a value of 10-6 m2/s. With this adjustment, the fission product releases the codes calculate at the edge of the compact corresponds to the release from the TRISO particles.

In PARFUME, the calculation of fission product transport through a collection of particles is weighted by the probability of the failure of these particles. The statistical variations in the modeling parameters of Table 4 are used in the thermomechanical stress analysis to determine any layer failure, at which point the diffusivity of that layer is set to 10-6 m2/s, corresponding to a loss of retentive capability. This relies on the strong assumption that a failed layer does not retain diffusing species at all, even partially, and it is implemented as such for lack of a better understanding of the diffusing mechanisms in failed layers. The resulting release from the collection of particles includes release from the driver fuel particles as well as release from the DTF particles.

To more accurately reproduce the number of particles with retentive and non-retentive coating layers, driver fuel particles and DTF particles were modeled separately. PARFUME has the capability to separately model driver fuel particles and DTF particles by decoupling the two particle types. PARFUME is run twice, once modeling the driver fuel particles with the IAEA diffusivities and once again with DTF particles, where it is assumed that the DTF particles fail early in irradiation and PyC layer diffusivities are set to 10-6 m2/s. This results in separate release fractions from driver fuel particles and DTF particles, which can then be combined accordingly in each compact for comparison to the measured release data. A similar approach was performed using BISON.

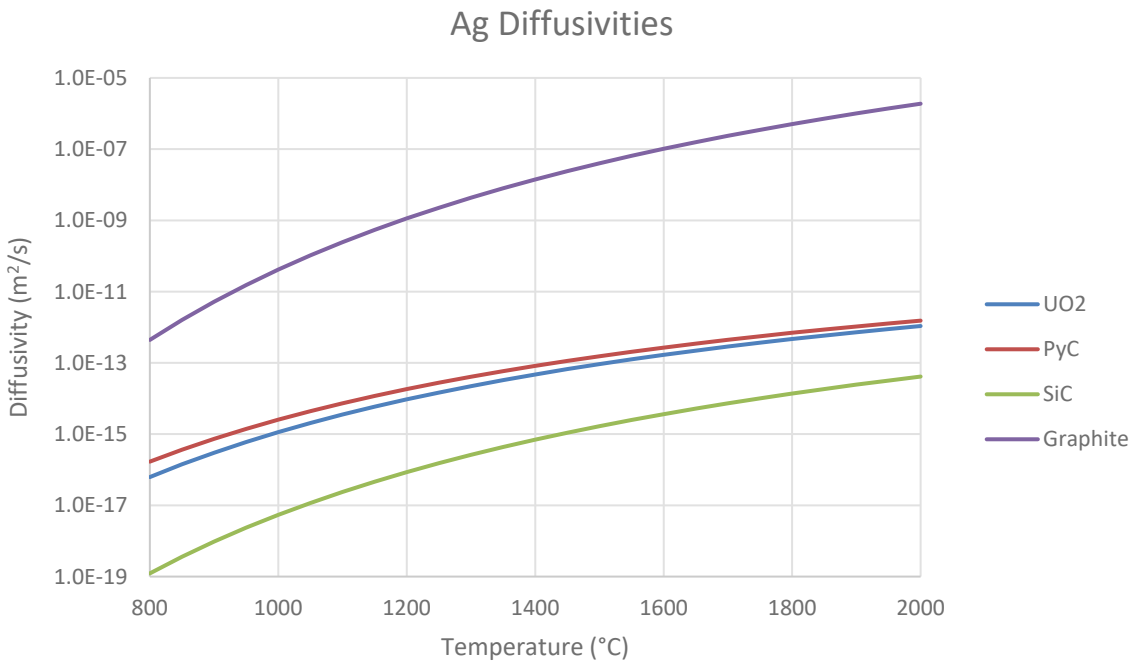

Figure 12. Silver diffusivities.

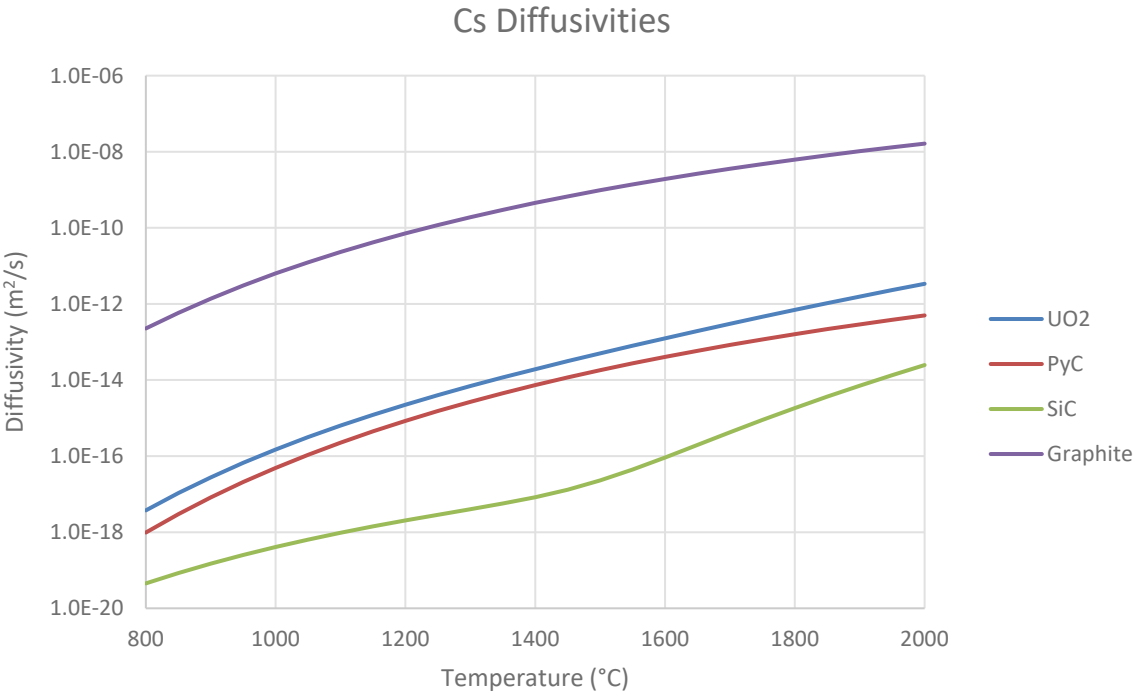

Figure 13. Cesium diffusivities.

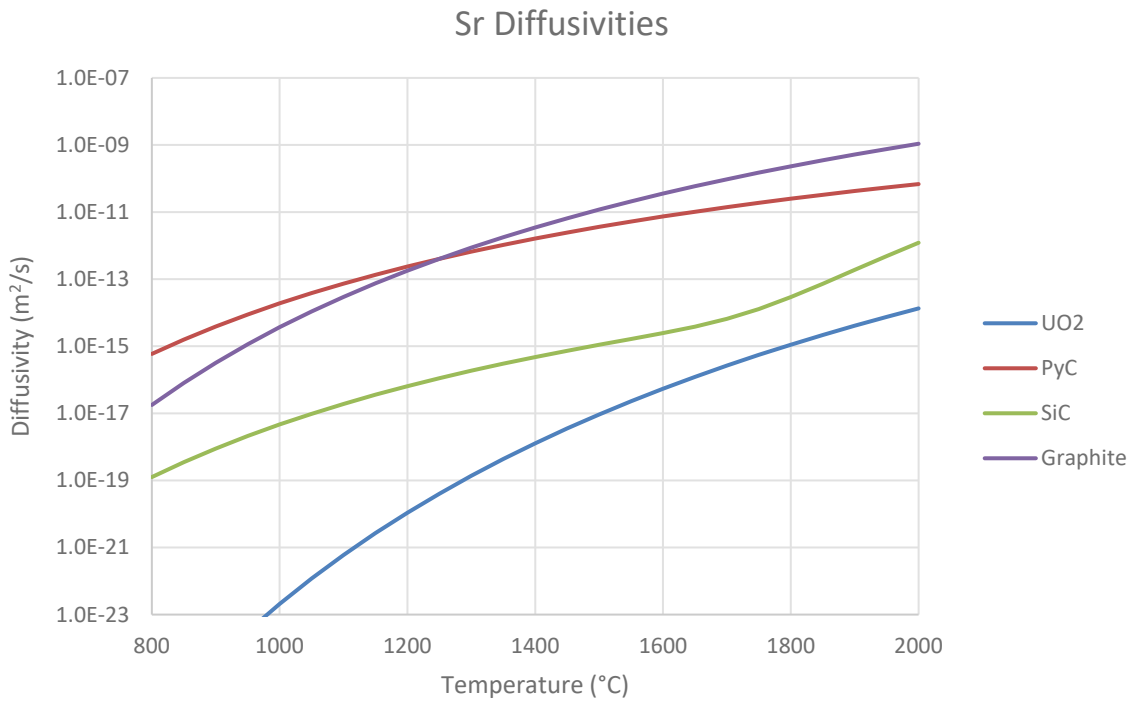

Figure 14. Strontium diffusivities.

4. RESULTS

Fission product release behavior during post-irradiation heating tests is complex and is dependent on fission product transport during irradiation. This includes the inventory that is released from DTF particles and driver fuel particles and the inventory of fission products held up in the OPyC layer and compact matrix at the end of irradiation. If the predicted distribution of retained fission products in the fuel at the end of irradiation differs substantially from the experiment, it could result in an appreciable difference between the predicted and measured heating test releases since the starting state of the fuel differs in the two cases. For example, release from a compact during a heating test may be dominated by inventory that was stored in the matrix at the end of irradiation. If the predicted release is dominated instead by release from intact driver fuel particles, then the fact that the dominant releases arise from different phenomena should be considered when comparing the experiment to the model.

The predicted release fraction results are highly dependent on fission product diffusivities that are used to model the irradiation and heating tests. One objective of the AGR program is to generate diffusivities that are more reflective of the current TRISO fuel. Updating the diffusivities for the kernel, particle layers, and compact matrix will result in a more accurate prediction from these models during irradiation. The more accurately these codes can predict the fission product inventory end state after irradiation, the less uncertainty there will be from the heat testing results. Ideally, the fission product inventory at the end of irradiation in the driver fuel particles, DTF particles and in the compact matrix would be experimentally quantified and available as an input into the model to more accurately predict the release during the heating tests. PIE work is currently being performed to obtain some of these data, which in turn can be used in the future to refine these fission product release predictions.

The measured heating test release fractions from selected as-irradiated AGR-3/4 fuel compacts were compared to the predicted fission product release fractions predicted by PARFUME and BISON for Ag-110m, Cs-134, and Sr-90. With the exception of Compact 8-2, the measured fission product release fractions are documented in a conference proceedings paper summarizing the results from the AGR-3/4 heating tests (Stempien, et al. 2018). As of this report's publication, the release fraction results from Compact 8-2 have not been formally documented. Although there is high confidence in the results from Compact 8-2 reported herein, the data should be considered preliminary. Since the heating test results for cesium are reported for the isotope Cs-134 and PARFUME does not distinguish between the individual cesium isotopes, the predicted results were multiplied by the decay-corrected mass fraction for Cs-134 obtained from the as-run neutronics calculations (Sterbentz 2015). These mass correction fractions are summarized in the fission product transport comparisons from the AGR-3/4 irradiation PIE and modeling predictions report previously published (Skerjanc and Jiang 2022).

4.1 Failure Probability

PARFUME is used to predict the probability of a population of particle failures to estimate the performance of the AGR-3/4 TRISO fuel during irradiation in ATR and then subsequently during heating tests in the FACS furnace. A key metric of fuel performance is the extent of fuel particle failure during normal operation and accident conditions. The number of fuel particle failures during normal reactor operation or under accident conditions can be used to characterize the quality of the fuel.

It is assumed that a fuel particle has failed when the SiC layer has become compromised and cracked, which leads to its inability to retain fission products. PARFUME was used to calculate the fuel particle failure probability due to the following failure mechanisms:

- Traditional pressure vessel failure
- Cracking of the IPyC layer
- Pressure vessel failures due to particle asphericity
- SiC layer attack by palladium (Pd).

A traditional pressure vessel failure is caused by a buildup of gases (e.g., fission gas, carbon monoxide). Stresses for this failure mechanism are determined using the one-dimensional solution in PARFUME for a three-layer (IPyC-SiC-OPyC) particle. Initially, the SiC layer is in compression due to shrinkage of the pyrolytic carbon layers. As the irradiation progresses, the SiC compressive stress becomes relaxed due to the pyrolytic carbon creep and the accumulation of fission gas. If the buildup of fission gas is significant, all the layers are put in tension which can lead to a pressure vessel failure of the TRISO particle. In general, the CO production in a UCO fuel particle is not significant enough to cause a nominal particle failure due to pressure (Ougouag and Jiang 2019) and it was not considered in the model.

Failure of the SiC layer caused by irradiation-induced shrinkage and the associated cracking of the IPyC layer is also considered in PARFUME. During irradiation, shrinkage of the initially intact IPyC layer induces a significant tensile stress in that layer. If the stress exceeds the tensile strength of the IPyC layer, then a radial crack develops in the IPyC. Because the shrinkage in the pyrocarbons dominates the particle behavior early during irradiation, large tensile stresses in the IPyC occur early. The presence of a crack in the IPyC layer creates a localized stress concentration in the SiC layer that could potentially lead to failure.

Another mechanism considered is pressure vessel failure that is impacted by particle asphericity. Aspherical particles have a flat facet created during fabrication but are otherwise spherical. During irradiation, the faceted portion of the particle acts as a flat plate that restrains the internal gas pressure. If the pressure reaches a high enough value, a local region of tensile stress develops in the central portion of the plate that can contribute to particle failures. Unlike failures caused by cracking of the IPyC, which is governed by shrinkage of the pyrocarbons, failures caused by asphericity are dominated by the internal pressure. Therefore, while failures due to IPyC cracking are predicted to occur early during irradiation when shrinkage stresses are at their highest, failures due to asphericity are likely to occur later when the internal pressure is highest.

Finally, chemical attack of the SiC layer by Pd is another failure mechanism considered and it is modeled in PARFUME by calculating the Pd penetration into the SiC layer. The penetration rate is calculated by an Arrhenius function fitted to all available in-reactor data for Pd penetration in SiC. Failure occurs when penetration through the SiC layer is complete, leading to the direct release of fission products. In actuality, the fuel particle would more than likely to fail prior to reaching a 100% Pd penetration (penetration through the entire SiC layer), and a limit can be applied to the fuel performance criteria to establish a bounding limit on Pd penetration.

Other failure mechanisms observed, but not explicitly modeled, include partial debonding of the IPyC from the SiC and fuel kernel migration into the SiC (observed historically but not in AGR fuel). In the case of IPyC/SiC debonding, the model assumes that the bond strength is relatively large (100 MPa) and IPyC-SiC debonding is not predicted by the codes. However, PIE of previous AGR experiments indicate that debonding does in fact occur suggesting that this assumption needs to be re-evaluated in future model improvements. As far as kernel migration due to temperature gradients, this effect is driven by the production of CO in UO_2 particles, and effect which is extremely limited in UCO particles, and is not expected to occur.

It is assumed that all DTF particles fail at the onset of irradiation in the fuel performance models. As for the driver fuel in the compacts, their time evolution failure probability histories are illustrated (Figure 15) covering both the irradiation experiment and their respective heating test. The failure probabilities shown in Figure 15 during irradiation are primarily due to failures associated with IPyC cracking. Failure probabilities driven by IPyC cracking occur early during irradiation since shrinkage of the pyrocarbons has the greatest effect. Referring to temperature profile in Figure 10, the ATR experienced a step change in power due to cycle change at approximately 50 EFPD. This resulted in a step change in temperature causing an increase in the probability of PyC cracking and subsequently total failure probability. After 50 days, internal particle pressure and creep counteract the tensile stress due to the shrinkage of pyrocarbon

layers resulting in no change to the failure probability associated with IPyC cracking. Only Compact 3-2 experienced an increase in fuel particle failure probability during the heating test. This was attributed to pressure vessel failures due to particle asphericity. The total fuel particle failure probability at the end of irradiation and heating tests were less than 2×10^{-7} for all fuel compacts which results in zero driver fuel particle failures, assuming 1,872 driver particles per compact. The fuel particle failure probability results predicted by PARFUME are summarized in Table 7. The SiC Pd penetration calculated by PARFUME for the compacts analyzed during the irradiation and heating test is summarized in Table 8. For all four compacts, the Pd penetration is less than one-third of the nominal SiC layer thickness (33.5 µm)

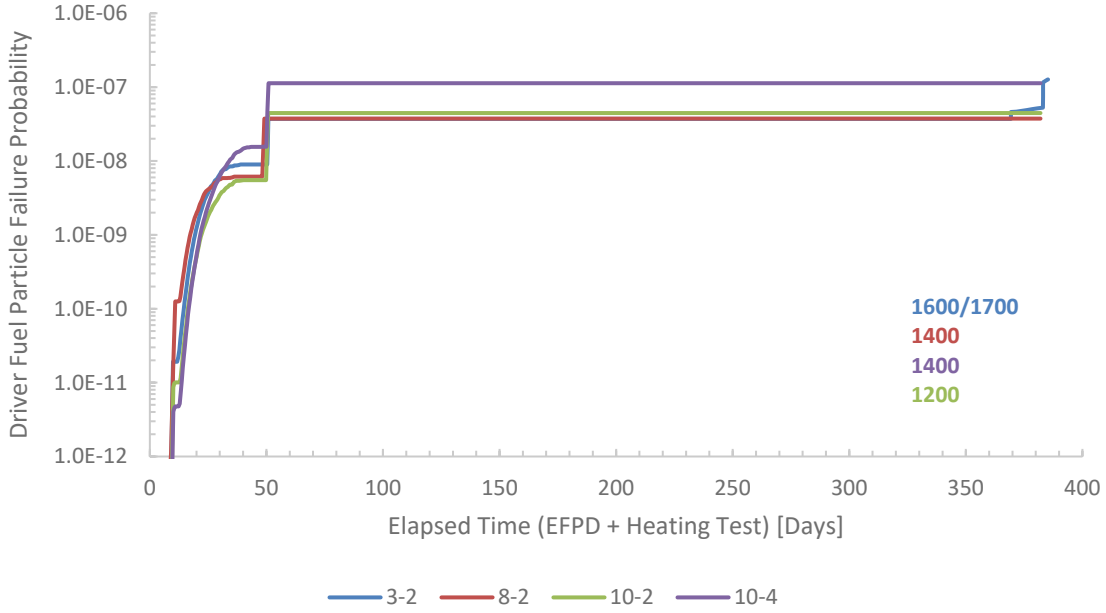

Figure 15. Driver fuel particle failure probability for selected AGR-3/4 compacts.

Table 7. Driver fuel particle failure probability for selected AGR-3/4 compacts

Compact	Irradiation			Heating Test			Total SiC Failure Probability
	Probability of			Probability of			
	SiC Failure	Failure due to		SiC Failure	Failure due to		
		IPyC Cracking	Pressure		IPyC Cracking	Pressure	
3-2	3.72E-08	3.72E-08	0.00E+00	8.97E-08	0.00E+00	8.97E-08	1.27E-07
8-2	3.75E-08	3.75E-08	0.00E+00	0.00E+00	0.00E+00	0.00E+00	3.75E-08
10-2	4.46E-08	4.46E-08	0.00E+00	0.00E+00	0.00E+00	0.00E+00	4.46E-08
10-4	1.13E-07	1.13E-07	0.00E+00	0.00E+00	0.00E+00	0.00E+00	1.13E-07

Table 8. Pd penetration for selected AGR-3/4 compacts

Compact	Pd Penetration (µm)	SiC Thickness (µm)
3-2	10.4	33.5
8-2	11.8	33.5
10-2	10.1	33.5
10-4	8.3	33.5

4.2 Compact 3-2 1600/1700°C Heating Test

The Compact 3-2 heating test temperature evolution and the measured fission product release fractions compared to predicted results from PARFUME and BISON are summarized in Figure 16. The measured Ag-110m is presented as a "low" and "high" estimate. In total, there were 31 plates exchanged during the heating test but only two had a measurable quantity of Ag-110m (Stempien, et al. 2018). The "low" estimate reflects only those two plates with measurable Ag-110m quantities and assumes that the other 29 plates did not contain any Ag-110m. The "high" estimate assumes that the 29 condensation plates without a measurable quantity of Ag-110m had an activity equal to the minimum detectable activity (MDA).

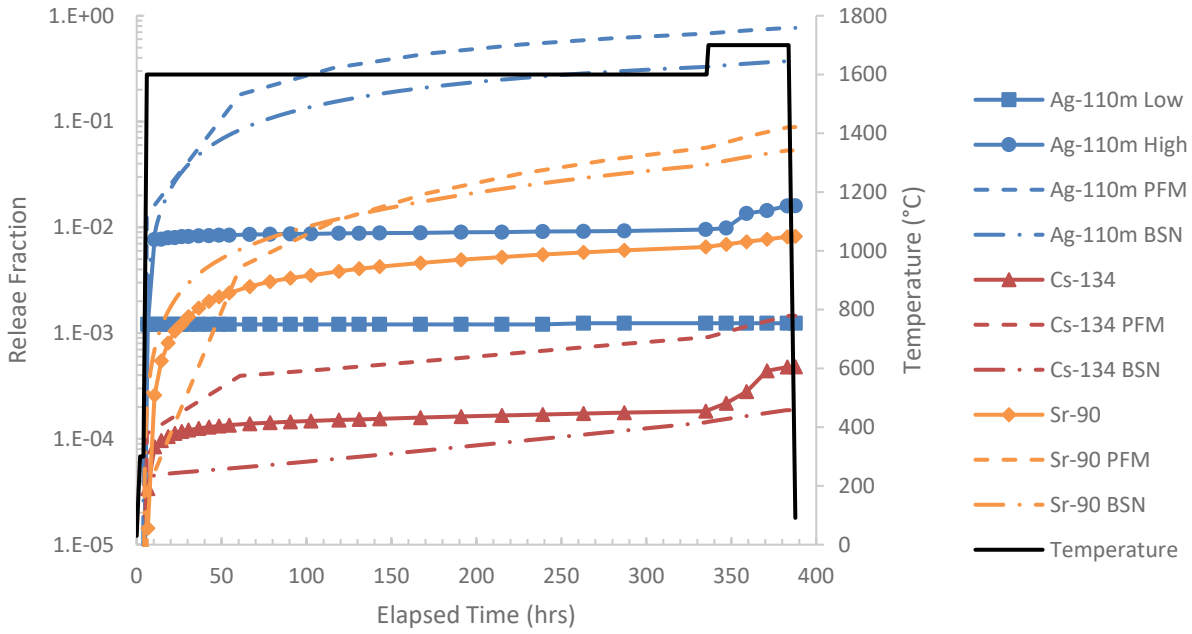

Figure 16. Compact 3-2 measured fission product release fraction versus PARFUME (PFM) and BISON (BSN) from the 1600/1700°C heating test.

The total measured and predicted fission product release fraction for the fission products of interest at the end of the heating test is summarized in Table 9 and illustrated in Figure 17. At the end of the heating tests, both PARFUME and BISON overpredict the release fraction for both Ag-110m and Sr-90. In the case of Ag-110m, the codes overpredict the low estimate value by approximately 2.5 orders of magnitude and 1.5 orders of magnitude of the high estimate. PARFUME overpredicts the Cs-134 release fraction while BISON underpredicts the end of the heating test measured value. Both codes overpredict the Sr-90 release fraction by approximately one-order of magnitude at the end of the heating test.

Table 9. Measured and predicted release fractions at the end of Compact 3-2 heating test.

Specie	Measured		PARFUME	BISON
	Low	High		
Ag-110m	1.24E-03	1.60E-02	7.68E-01	3.72E-01
Cs-134	4.84E-04		1.46E-03	1.87E-04
Sr-90	8.32E-03		8.86E-02	5.32E-02

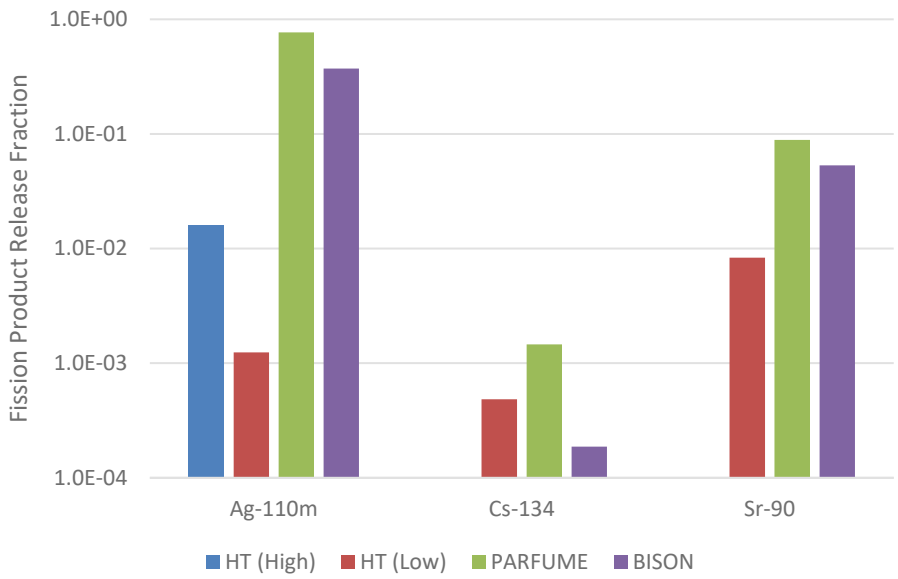

Figure 17. End of the heating test measured release fractions (HT) versus the predicted release fractions for Compact 3-2.

4.3 Compact 8-2 1400°C Heating Test

The Compact 8-2 heating test temperature evolution and the measured fission product release fractions compared to predicted results from PARFUME and BISON are summarized in Figure 18. In total, there were 19 condensation plates exchanged during the heating test. Similar to Compact 3-2, some of the condensation plates did not have a measurable quantity of Ag-110m and the low estimate assumes those plates did not contain any Ag-110m. The high estimate assumes the condensation plates that did not have any Ag-110m had the MDA. It should be noted that the experimental results presented below have not been publicly documented and the data should be treated as preliminary until they have been formally published. However, when the results from Compact 8-2 are compared to the other three compacts in this study, it can be concluded that there is high confidence in these results and that they may only slightly differ from the published values when they become available.

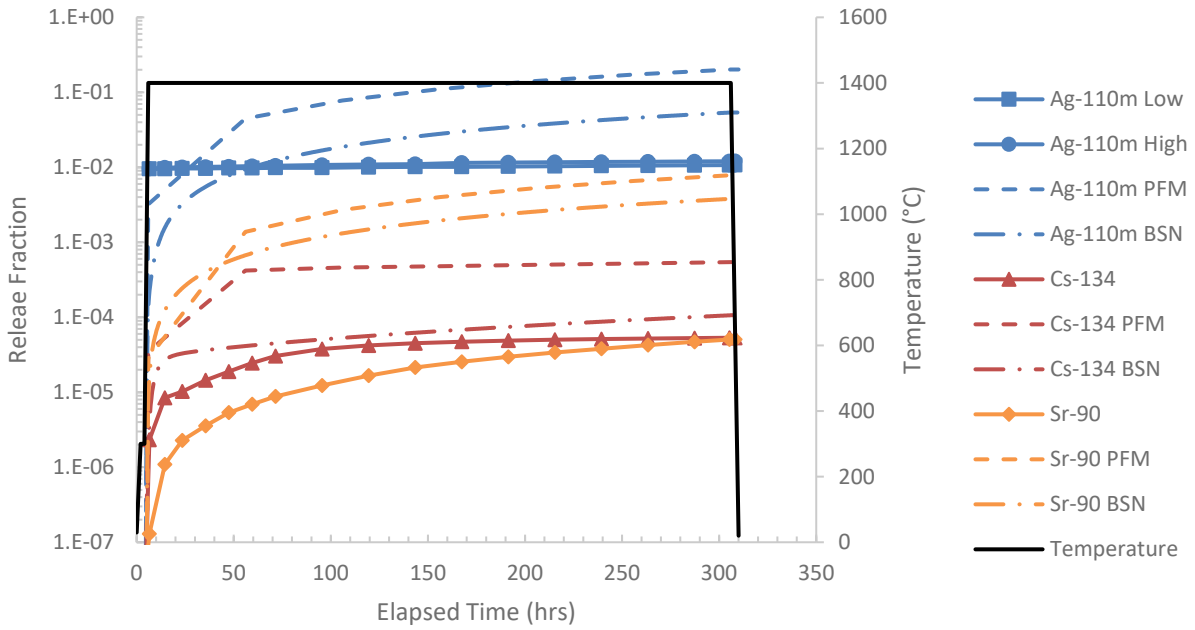

Figure 18. Compact 8-2 measured fission product release fraction versus PARFUME (PFM) and BISON (BSN) from the 1400°C heating test.

The total measured and predicted fission product release fraction for the fission products of interest at the end of the heating test is summarized in Table 10 and illustrated in Figure 19. Both PARFUME and BISON overpredict the Ag-110m, Cs-134, and Sr-90 release fractions when compared to the measured values at the end of the heating test. In the case of Sr-90, the codes overpredict the measured release fraction by approximately two-orders of magnitude.

Table 10. Measured and predicted release fractions at the end of Compact 8-2 heating test.

Specie	Measured		PARFUME	BISON
	Low	High		
Ag-110m	1.07E-02	1.21E-02	2.02E-01	5.38E-02
Cs-134	5.33E-05		5.44E-04	1.06E-04
Sr-90	5.07E-05		7.85E-03	3.80E-03

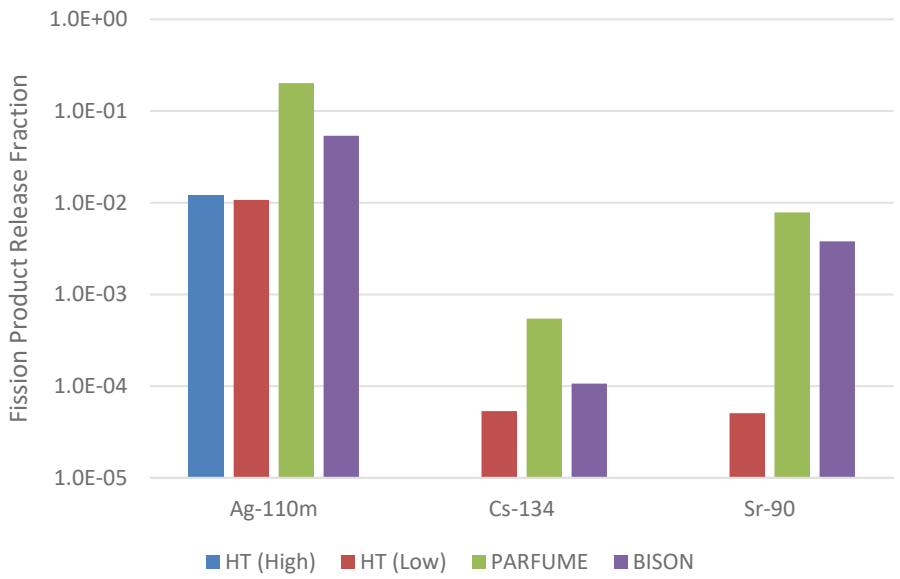

Figure 19. End of the heating test measured release fractions (HT) versus the predicted release fractions for Compact 8-2.

4.4 Compact 10-2 1200°C Heating Test

The Compact 10-2 heating test temperature evolution and the measured fission product release fractions compared to predicted results from PARFUME and BISON are summarized in Figure 20. During the heating test of Compact 10-2, 18 of the 19 condensation plates contained a measurable quantity of Ag-110m so a "low" and "high" estimate is not necessary (Stempien, et al. 2018).

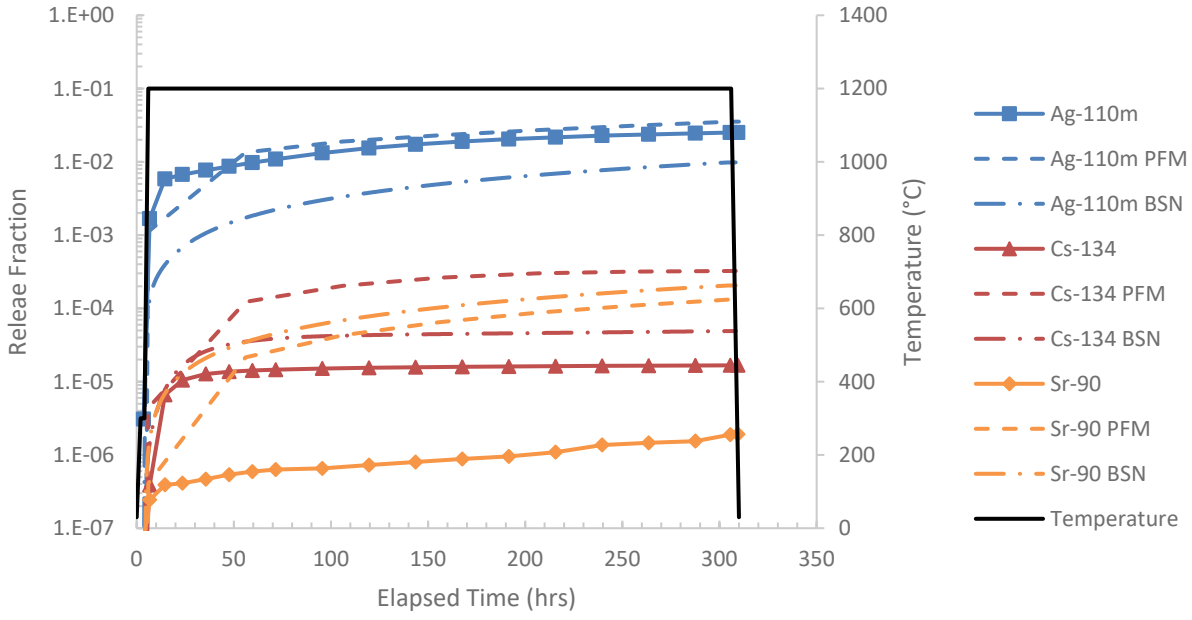

Figure 20. Compact 10-2 measured fission product release fraction versus PARFUME (PFM) and BISON (BSN) from the 1200°C heating test.

The total measured and predicted fission product release fraction for the fission products of interest at the end of the heating test are summarized in Table 11 and illustrated in Figure 21. At the end of the heating test, the measured and predicted silver release fractions from PARFUME and BISON were in fairly good agreement. However, both PARFUME and BISON overpredicted the release fractions for Cs-134 (by approximately one order of magnitude) and Sr-90 (two orders of magnitude). Although Compacts 10-2 and 8-2 experience different daily temperatures, their TAVA temperatures were the same (1213°C). As discussed previously in Section 3.2, at the end of irradiation, their in-pile Ag release fraction differed between the compacts even though their final TAVA temperatures were the same. Regardless, the release fractions from these two compacts at different heating test temperatures can be compared to evaluate what impact the heating test temperature has on compacts that experienced relatively the same in-pile irradiation thermal conditions. In addition, since Compact 10-2 heating test temperature (1200°C) and the irradiation TAVA temperature (1213°C) are similar, the fission product release rates can be compared to provide further analysis. These analyses will be discussed further in Section 5.

Table 11. Measured and predicted release fractions at the end of Compact 10-2 heating test.

Specie	Measured	PARFUME	BISON
Ag-110m	2.51E-02	3.53E-02	9.82E-03
Cs-134	1.67E-05	3.24E-04	4.90E-05
Sr-90	1.92E-06	1.33E-04	2.05E-04

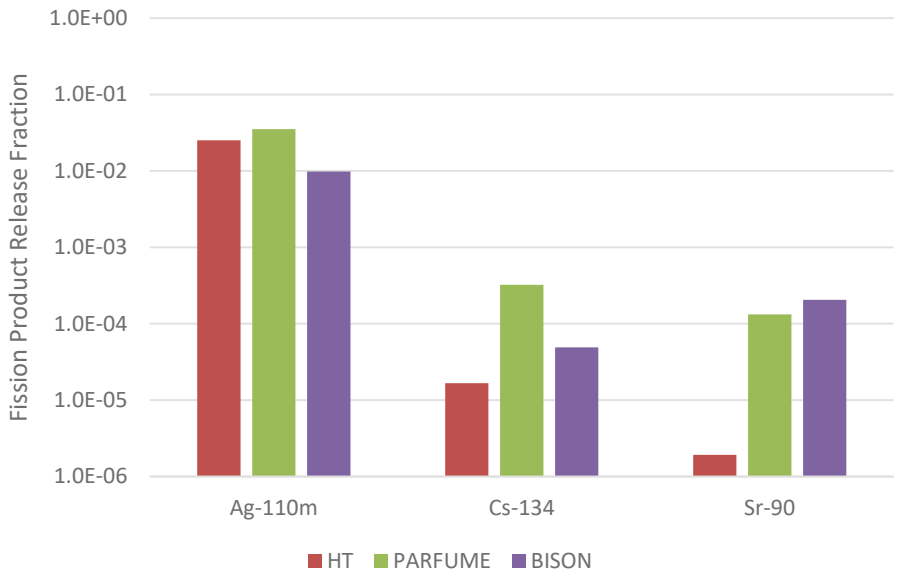

Figure 21. End of the heating test measured release fractions (HT) versus the predicted release fractions for Compact 10-2.

4.5 Compact 10-4 1400°C Heating Test

The Compact 10-4 heating test temperature evolution and the measured fission product release fractions compared to predicted results from PARFUME and BISON are summarized in Figure 22. As with Compact 3-2 and 8-2, some of the condensation plates from the Compact 10-4 heating test did not contain a measurable quantity of Ag-110m and the same methodology was applied that was previously discussed to obtain a high and a low estimate (Stempien, et al. 2018).

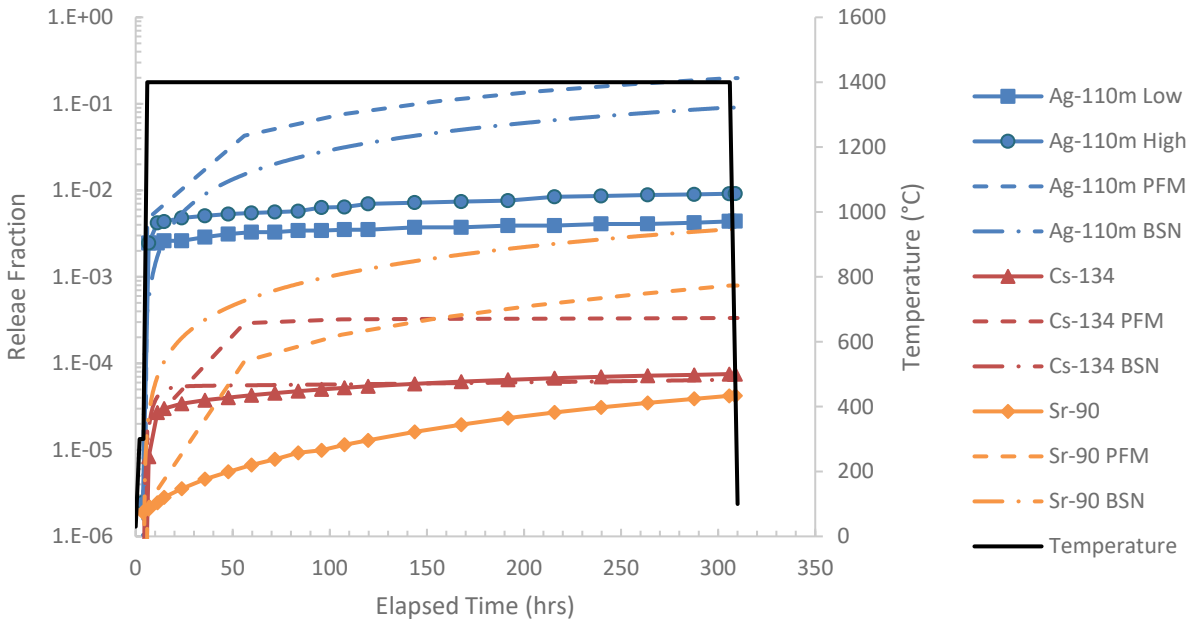

Figure 22. Compact 10-4 measured fission product release fraction versus PARFUME (PFM) and BISON (BSN) from the 1400°C heating test.

The total measured and predicted fission product release fraction for the fission products of interest at the end of the heating test is summarized in Table 12 and illustrated in Figure 23. Again, PARFUME and BISON overpredict the Ag-110m and Sr-90 release fractions. The BISON-predicted release fraction for Cs-134 was in good agreement with the measured release fraction while PARFUME overpredicted the measured results. Since Compact 10-4 and 8-2 have the same heating test temperature (1400°C) and evolution, the fission product release results from these two compacts can be compared to analyze the effect the irradiation temperature has on subsequent release rates.

Table 12. Measured and predicted release fractions at the end of Compact 10-4 heating test.

Specie	Measured		PARFUME	BISON
	Low	High		
Ag-110m	4.40E-03	9.14E-03	1.98E-01	9.05E-02
Cs-134	7.51E-05		3.34E-04	6.46E-05
Sr-90	4.22E-05		7.93E-04	3.53E-03

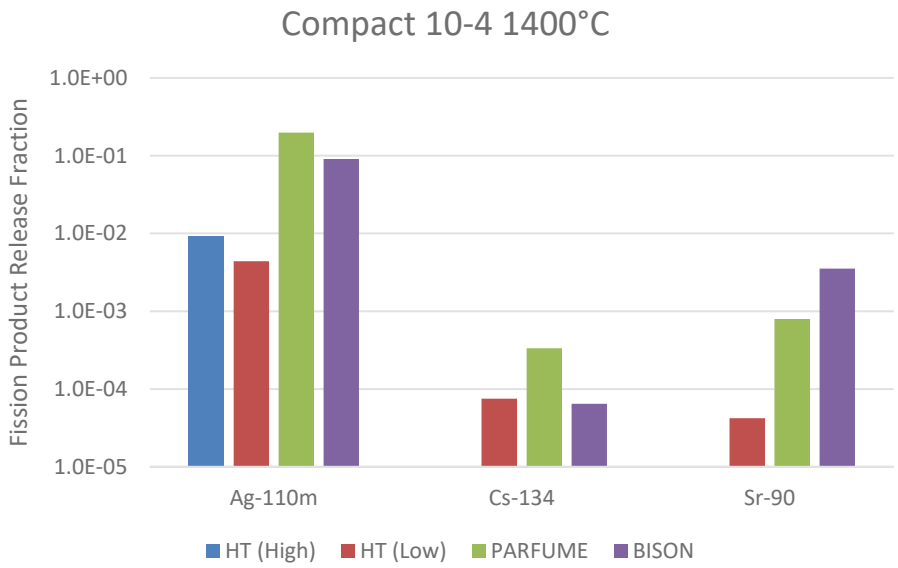

Figure 23. End of the heating test measured release fractions (HT) versus the predicted release fractions for Compact 10-4.

5. ANALYSIS AND DISCUSSION

The results presented in the previous section are discussed in more detail in the following sections to provide further comparisons on a compact- and temperature-level basis. This includes fission product release of silver, cesium, and strontium as well as a comparison between Compacts 8-2 and 10-4 since they have the same heating test temperature but experienced different TAVA temperatures during irradiation. In addition, a comparison between compacts 8-2 and 10-2 is provided since they have the same TAVA irradiation temperature but different temperature histories leading to those identical TAVA temperatures and different heating test temperatures (1400°C and 1200°C, respectively.

5.1 Silver Release

The heating test release fraction data correspond to the amount of silver released from the compacts and measured during the entire duration of the heating tests. Similar to AGR-1 and AGR-2, it is postulated that the silver released during approximately the first 24 hours of the tests is believed to be predominantly silver retained in the matrix and possibly the OPyC at the end of irradiation phase (Morris, et al. 2014). Since AGR-3/4 contain DTF particles, it is possible that some of the prompt silver release is not entirely from the matrix inventory but rather from residual inventory from DTF particles, However, the prompt release of silver when the compacts are heated to high temperature, followed by a more gradual release, tends to indicate that the early release is not from the particles but rather from the matrix.

The measured and predicted silver release fraction evolution for the selected compacts is illustrated in Figure 24. With the exception of the BISON prediction for Compact 10-2, both codes over-predicted total silver release fraction, as illustrated in Figure 25 and summarized in Table 13. The predicted silver release during the heating test is primarily from intact driver fuel particles since it is assumed that most of the silver from the DTF particles was released in-pile during the irradiation and the inventory stored in the matrix is relatively small. Experimentally however, the data indicate that the measured Ag release is from inventory in the compact matrix at the beginning of the heating tests suggesting that the model and empirical release fraction data are derived from different phenomenon. The overpredictions observed in Figure 24 and Figure 25 indicate that the diffusivity in the SiC is significantly overestimated because of the release from driver particles is largely overpredicted.

Compact gamma scanning has been performed to measure the retained silver fraction in the compacts (Harp, Stempien and Demkowicz 2021). These values are summarized in Table 14 along with the predicted retained silver fraction (1 – release fraction) from PARFUME and BISON. Values from Table 14 show PARFUME and BISON underpredict the release fraction (overpredict the retention fraction) when compared to the measured values from the compact gamma scan at the end of irradiation. The underprediction by PARFUME and BISON results in more silver being available to be released during the heating tests. For example, at the end of irradiation of AGR-3/4, it is estimated that Compact 3-2 retained approximately 7% of the predicted Ag-110m produced while PARFUME and BISON predict an Ag-110m retention fraction of 74% and 84%, respectively. This initial difference could explain why the silver release fraction predicted by PARFUME and BISON during the heating tests are higher than the measured values from the FACS condensation plates in addition to the higher diffusivities in the codes.

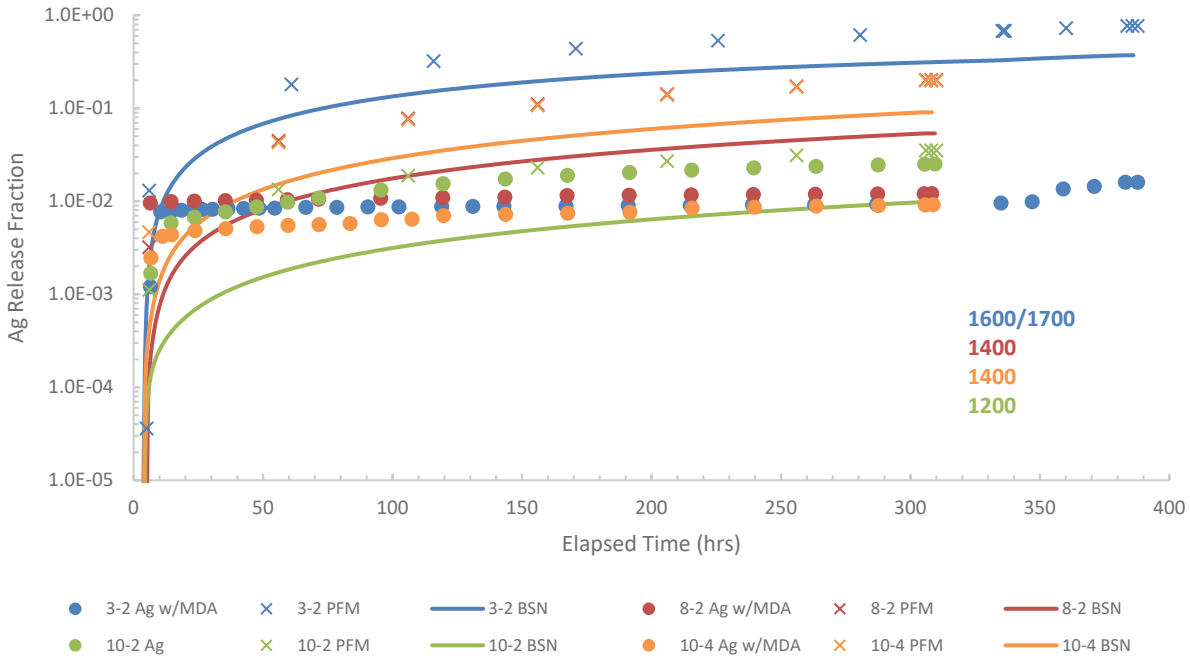

Figure 24. Measured silver (Ag-110m) release fraction evolution versus PARFUME (PFM) and BISON (BSN).

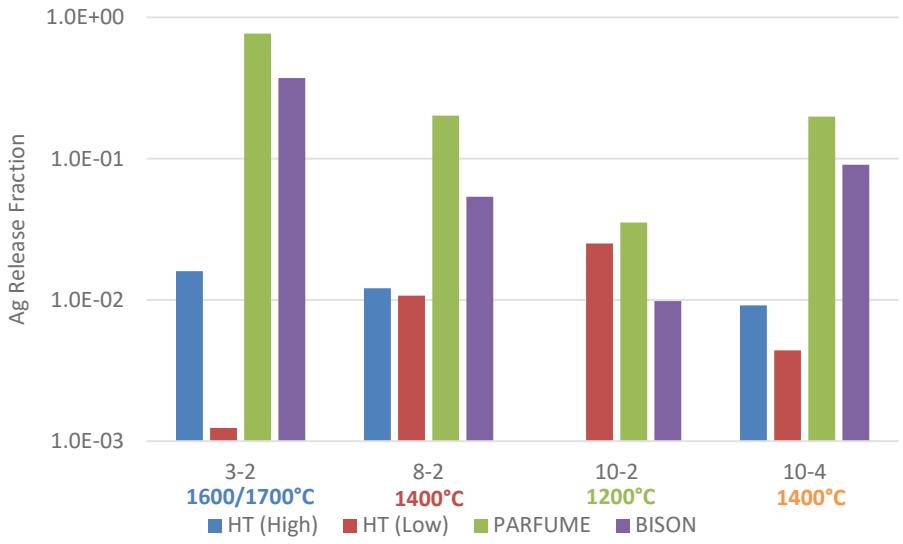

Figure 25. End of the heating test measured silver (Ag-110m) release fractions (HT) versus the predicted release fractions.

Table 13. Measured and predicted silver (Ag-110m) release fractions at the end of the heating tests.

Compact	Measured		PARFUME	BISON
	Low	High		
3-2	1.24E-03	1.60E-02	7.68E-01	3.72E-01
8-2	1.07E-02	1.21E-02	2.02E-01	5.38E-02
10-2	2.51E-02		3.53E-02	9.82E-03
10-4	4.40E-03	9.14E-03	1.98E-01	9.05E-02

Table 14. Measured and predicted silver (Ag-110m) retention fraction at the end of the AGR-3/4 irradiation.

Compact	Measured	PARFUME	BISON
3-2	7%	74%	84%
8-2	14%	44%	66%
10-2	20%	65%	79%
10-4	5%	78%	87%

Regardless of the Ag-110m initial inventory at the beginning of the heating tests, the release fraction rate provides insight into how well the two codes predict fission product transport through particles and compact matrix. Figure 26 illustrates the measured and predicted silver release fraction rates on a compact level basis during the heating test evolution. Since the measured silver release fraction of some of the compacts were only observed on a couple of plates, the Ag-110m release fraction rates illustrated in Figure 26 represent a high and low estimate using the methodology previously discussed. The low data series use open square symbols to denote the times when Ag was actually detected, and the high data series use MDAs to provide an upper-bound estimate on the rates at times where no Ag was detected. As expected, the silver release fraction rate is higher during the temperature ramp and decreases throughout the heating tests. Again, the BISON release fraction rate for Compact 10-2 is the only release fraction rate prediction that is lower than the measured rate. The silver release fraction rate from both codes increased during the temperature ramp from 1600°C to 1700°C for Compact 3-2 and decreased until the end of the heating test. The results in Figure 26 indicate the SiC diffusivities in the two codes are overestimated resulting in an overprediction of the Ag-110m release fraction rate from the driver fuel.

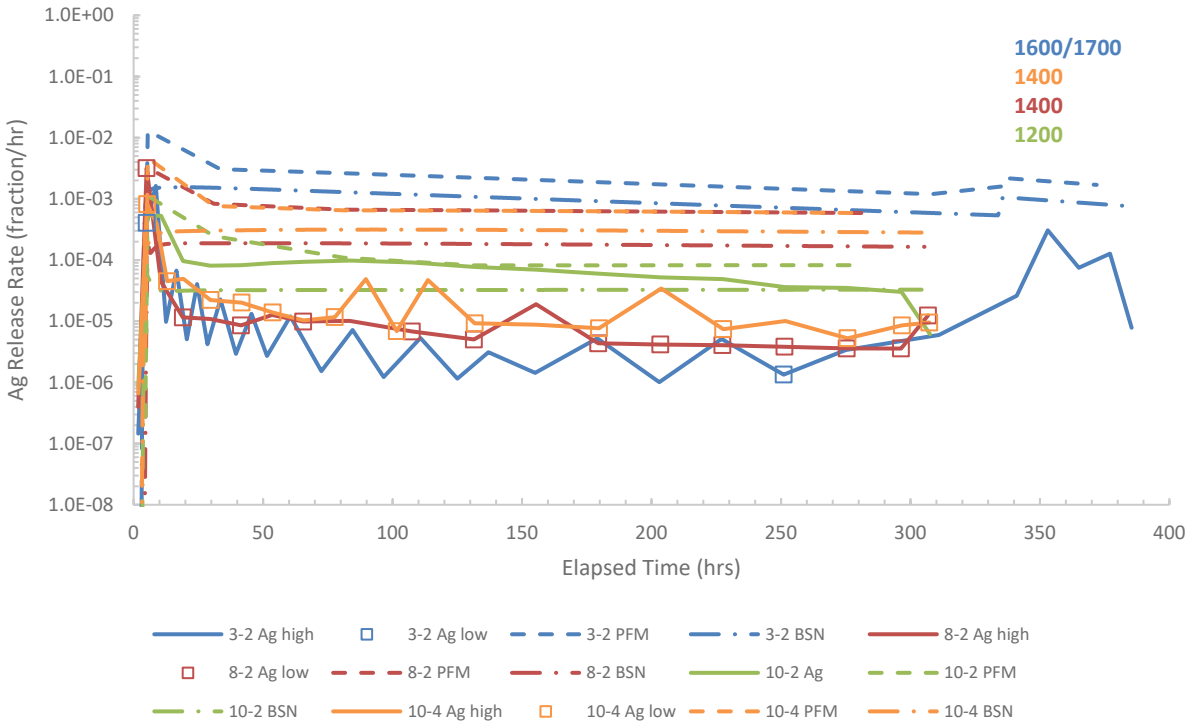

Figure 26. Measured silver (Ag-110m) release fraction rate evolution versus PARFUME (PFM) and BISON (BSN).

5.2 Cesium Release

Measured cesium released fraction, specifically Cs-134, from the compacts during the heating tests were compared to the predicted values from PARFUME and BISON on a compact level basis as illustrated in Figure 27. PARFUME overpredicts the cesium release in all four compacts while BISON overpredicts the cesium release in Compacts 8-2 and 10-2. As shown in Figure 27, the measured and predicted cesium release fraction was fairly consistent throughout the irradiation and is bound by two-orders of magnitude (between $10^{-3} – 10^{-5}$). The measured and predicted release increased with increasing heating test temperatures, which is to be expected by the models. The Cs-134 release fractions for the four compacts at the end of their respective heating tests are summarized in Figure 28 and Table 15.

Both models predict the more than 99% of the cesium from DTF particles will be released during the irradiation leaving little inventory to be released during heating tests. In addition, PARFUME predicts zero driver fuel particle failures, therefore, the cesium release fraction results from the codes are primarily due to diffusional fission product transport from intact driver fuel particles since most of the cesium from DTF particles is predicted to have been released. Further, it has previously been speculated that any U or Cs-134 measured in the OPyC or compact matrix with non-retentive SiC or complete particle failures can be attributed to the as-fabricated uranium contamination (Morris, et al. 2014). This would result in the measured release from intact driver fuel particles to be even lower than those presented in Figure 28, magnifying the overprediction from PARFUME and resulting in BISON overpredicting all four compacts. In addition, since both codes predict nearly complete release of Cs-134 from the DTF particles during irradiation, it is possible that not all Cs-134 from DTF particles was released in-pile. The models do not capture this available inventory and the cesium release results observed between the experiment and the two codes do not compare the same fission product release phenomena.

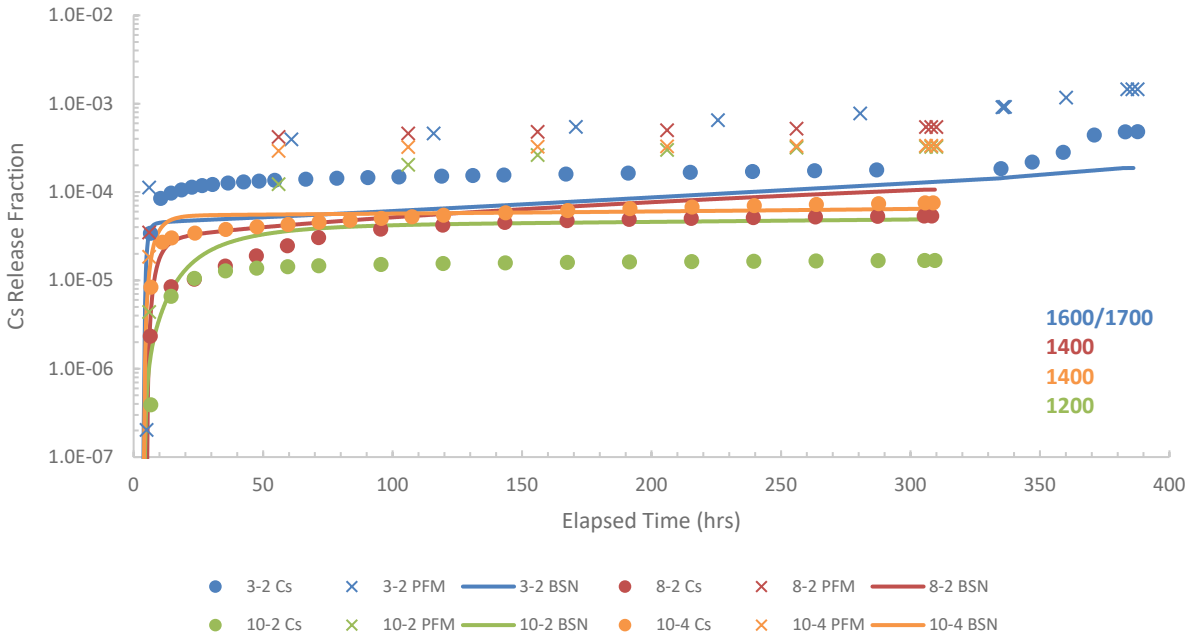

Figure 27. Measured cesium (Cs-134) release fraction evolution versus PARFUME (PFM) and BISON (BSN).

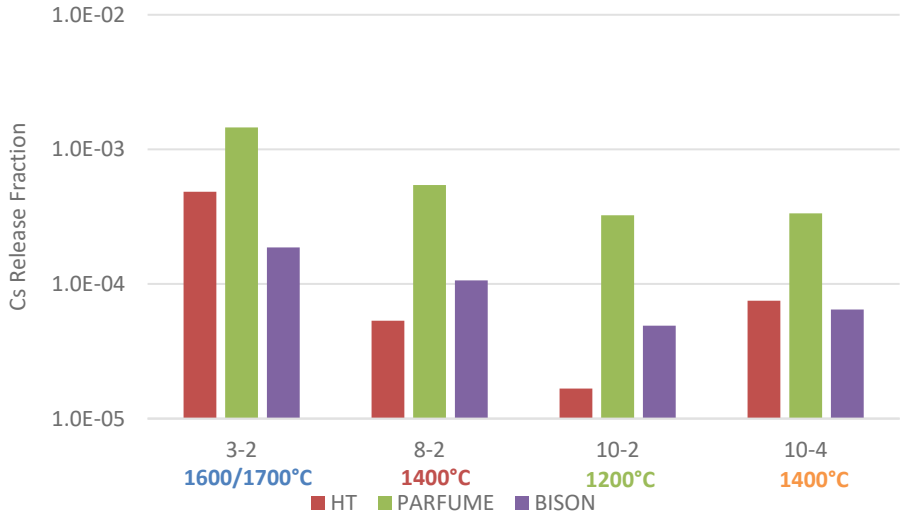

Figure 28. End of the heating test measured cesium (Cs-134) release fractions (HT) versus the predicted release fractions.

Table 15. Measured and predicted cesium (Cs-134) release fractions at the end of the heating tests.

Compact	Measured	PARFUME	BISON
3-2	4.84E-04	1.46E-03	1.87E-04
8-2	5.33E-05	5.44E-04	1.06E-04
10-2	1.67E-05	3.24E-04	4.90E-05
10-4	7.51E-05	3.34E-04	6.46E-05

The measured and predicted cesium release fraction rate is illustrated in Figure 29 for all four compacts. Similar to the measured release fraction, the measured release fraction rate increases with heating test temperature. This is not necessarily the case with PARFUME. Compact 10-2 (1200°C) initially has a lower release fraction rate than Compacts 8-2 and 10-4 (1400°C) but after approximately 60 hours, the release fraction rate becomes higher. It is speculated that this can be attributed to more cesium inventory available to be released in Compact 10-2. When compared to Compact 10-4, it remains higher throughout the remainder of the heating test. At approximately 210 hours, the predicted release fraction rate from Compact 8-2 eventually overcomes Compact 10-2 and remains higher for the remainder of the heating test.

Another observation from Figure 29 includes the fact that after the initial ramp, the measured cesium release fraction rate decreases throughout the remainder of the test (excluding the heat up ramp to 1700°C for Compact 3-2). This is not necessarily the case with PARFUME and BISON for Compacts 3-2, 8-2, and 10-4. For example, the predicted cesium release fraction rate from the two codes for Compact 3-2, after decreasing post initial heat up, increases until the end of the heating test, even after the 1600/1700°C jump.

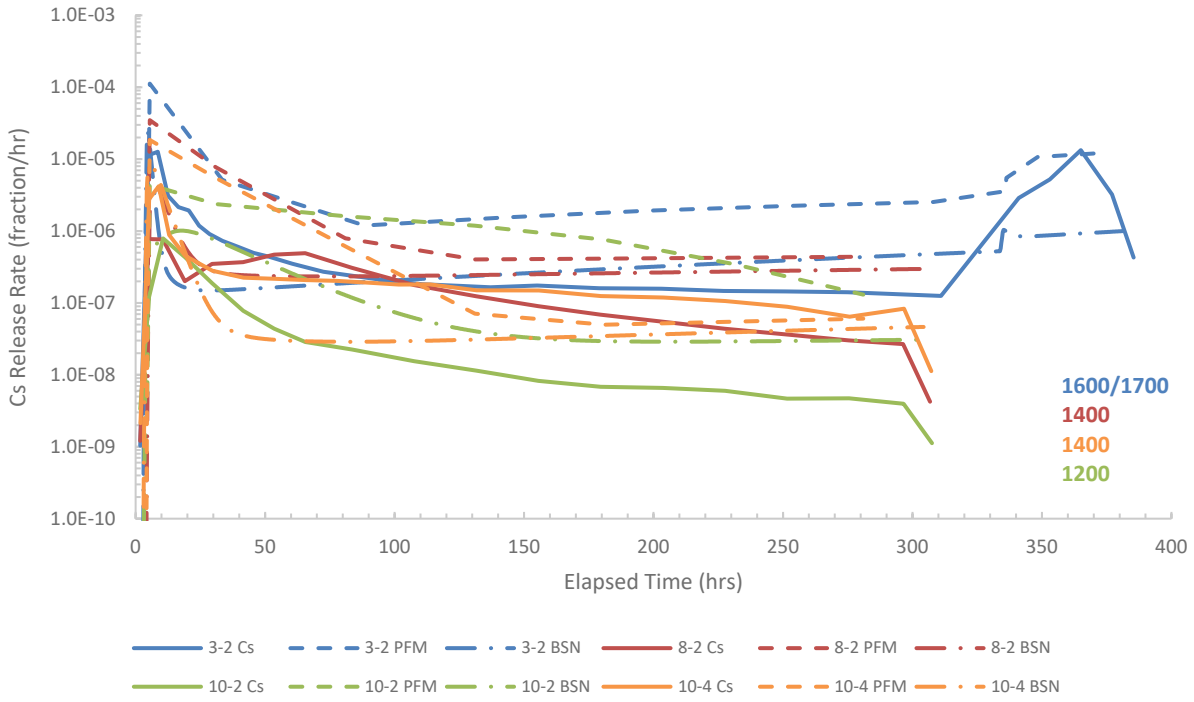

Figure 29. Measured cesium (Cs-134) release fraction rate evolution versus PARFUME (PFM) and BISON (BSN).

Based on the cesium release fraction and release fraction rates, both modeling codes appear to overestimate the cesium diffusivity. A previous study based on the AGR-1 heating tests indicate that this can be attributed to an overestimation of the diffusivities in both the UCO kernel and the SiC layer (Collin 2014). In the case of the UCO kernel, this overestimation can be as high as 10^2 to 10^3. For the SiC layer, the diffusivity overestimation can be ten times higher at 1600°C and 10^3 times higher at 1700°C. Based on these results from the AGR-3/4 heating tests of as-irradiated compacts, the cesium release fraction from the modeling codes are overestimating the measured values consistent with the data from the AGR-1 heating test.

5.3 Strontium Release

The measured and predicted strontium (Sr-90) time evolution release fractions for the selected compacts is illustrated in Figure 30. Again, the measured and predicted strontium release fractions increased with increasing heating test temperatures. The predicted values from BISON for the compacts heat tested at 1400°C were similar (although BISON overpredicts the measured values by approximately two-orders of magnitude) whereas PARFUME predicts a strontium release fraction approximately one-order of magnitude higher for Compact 8-2 when compared to Compact 10-4 throughout the heating test even though they were at the same temperature. Without knowing the source of the Sr-90 (DTF particles, driver particles, or compact matrix hold up), it is difficult to speculate the reason for this discrepancy calculated by PARFUME. The PARFUME- and BISON-predicted strontium release fractions for Compacts 3-2 and 10-2 were in fairly good agreement with each other but both codes overpredicted the measured release fractions. The measured and model-predicted strontium release fractions at the end of the heating tests for the capsules are summarized in Figure 31 and Table 16.

Unlike silver and cesium, both codes predict that not all the strontium inventory from DTF particles will be released during the irradiation. The predicted strontium release fraction from DTF particles after irradiation by PARFUME vary between 0.2% (Compact 10-4) to 5.6% (Compact 8-2) leaving a substantial inventory of strontium available for release during the heating tests. It is not possible to determine directly if the strontium release measured during heat testing is due to release through intact driver fuel particles, DTF particles, or simply from residual inventory in the compact matrix at the end of irradiation from both driver and DTF particles. Previous PIE data, however, suggests that the majority of the strontium release from heat testing is due to inventory residing in the compact matrix at the end of irradiation (Morris, et al. 2014); it is just impossible to determine if that inventory is from driver or DTF particles.

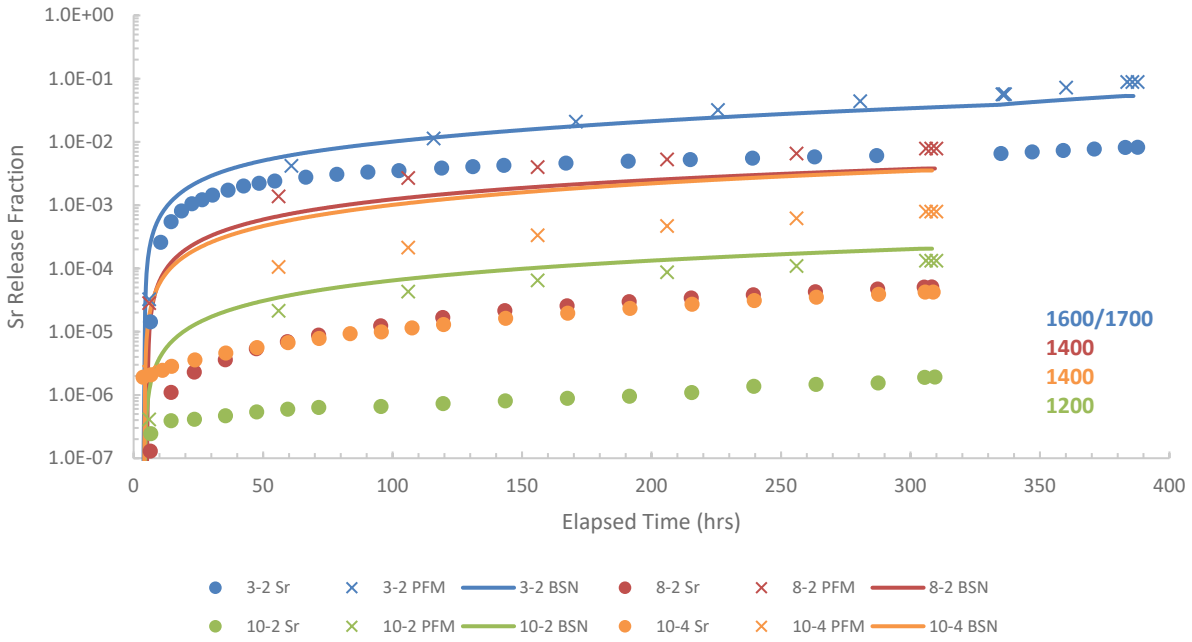

Figure 30. Measured strontium (Sr-90) release fraction evolution versus PARFUME (PFM) and BISON (BSN).

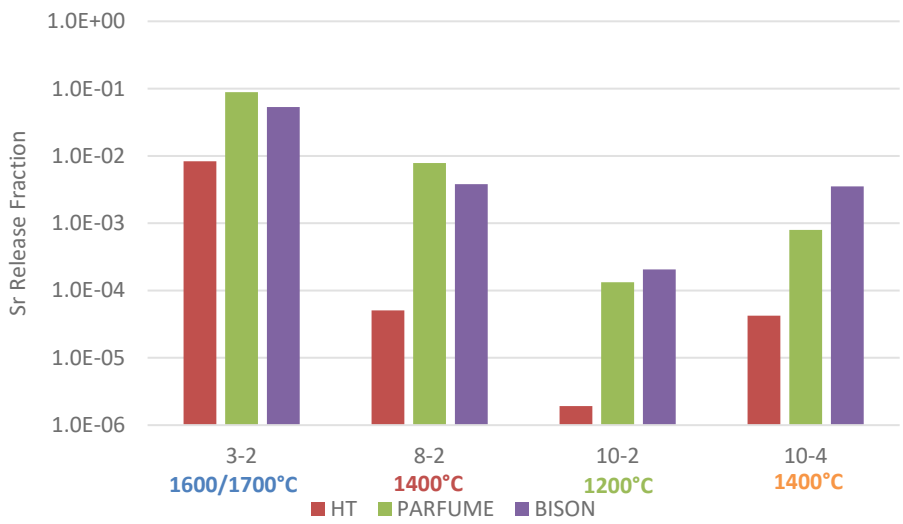

Figure 31. End of the heating test measured strontium (Sr-90) release fractions (HT) versus the predicted release fractions.

Table 16. Measured and predicted strontium (Sr-90) release fractions at the end of the heating tests.

Compact	Measured	PARFUME	BISON
3-2	8.32E-03	8.86E-02	5.32E-02
8-2	5.07E-05	7.85E-03	3.80E-03
10-2	1.92E-06	1.33E-04	2.05E-04
10-4	4.22E-05	7.93E-04	3.53E-03

The measured and predicted strontium (Sr-90) release fraction rates are summarized in Figure 32. The measured strontium release fraction rates and the predicted rates from PARFUME and BISON were relatively constant throughout the heating tests after the initial heat-up ramp, with the exception of the temperature jump in Compact 3-2 from 1600°C to 1700°C. Even after the temperature increase, the release rate in Compact 3-2 was relatively constant. Similar to the release fraction temperature evolution, the release fraction rate increases with increasing heat test temperature. The predicted release rate from BISON for Compacts 8-2 and 10-4 were relatively the same, which is expected since they both had the same heating test temperature. This is also true for the measured release fraction rate for these two compacts. The same cannot be said about the PARFUME prediction, where the predicted release rate for Compact 8-2 is higher than Compact 10-4 by approximately one-order of magnitude. This is consistent with the overall release fraction time evolution predicted by PARFUME illustrated in Figure 30 and as previously stated, without knowing the source of the Sr-90 release, the complexity of the AGR-3/4 experiment makes it difficult to determine why the predicted release rate by PARFUME is higher for Compact 8-2 when compared to Compact 10-4 even though they were held at the same isothermal temperature.

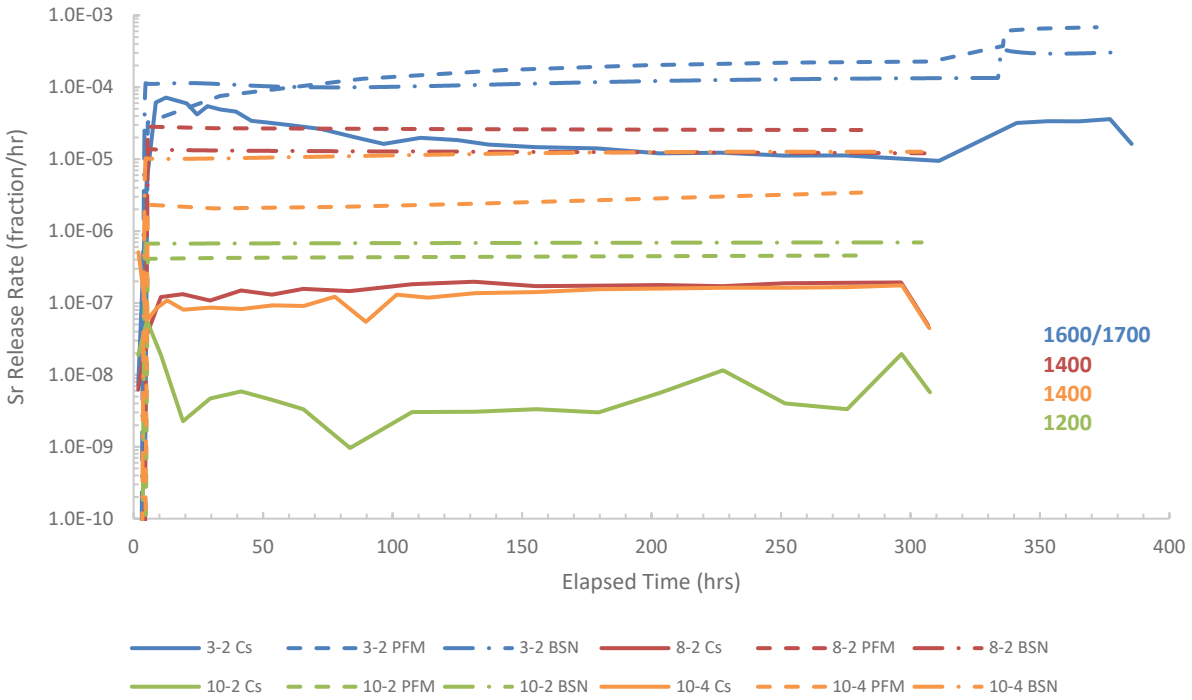

Figure 32. Measured strontium (Sr-90) release fraction rate evolution versus PARFUME (PFM) and BISON (BSN).

Comparisons between the two modeling codes and the strontium release measurements indicate that the strontium diffusivities are overestimated in PARFUME and BISON. The overestimation of diffusivities can either be in the UCO kernel, SiC layer, matrix, or possibly all three. Since the majority of the strontium inventory from DTF particles were not predicted to be released during irradiation, individual contributions to the measured strontium release from inventory in intact driver particles, DTF particles, and the compact matrix cannot be distinguished, making comparison of the model and empirical data difficult. PIE results (data currently being analyzed and will be published at a later date) may provide information concerning the post-irradiation inventory of fission products in the matrix and DTF kernels that can help better understand the heating test releases. Based on these limitations, it is not possible to properly assess the overestimation of the strontium diffusivities used in the codes.

5.4 Compacts 8-2 and 10-4

Compacts 8-2 and 10-4 were compared on a compact basis since they both experienced a heating test temperature of 1400°C. Although the heating test temperature was the same, the compact experienced different irradiation conditions, as summarized in Table 17. Compact 8-2 had a higher fluence and burnup level and experienced a higher TAVA temperature when compared to Compact 10-4. This will result in higher fission product production in Compact 8-2 but also higher fission product release during irradiation leaving less inventory to be released during the heating test.

Table 17. Irradiation conditions and heating test temperature for Compacts 8-2 and 10-4.

Compact	Fluence (10^{25} n/m^2)	Burnup (%FIMA)	TAVA Irradiation Temp. (°C)	Heating Test Temp. (°C)
8-2	5.11	14.58	1213	1400
10-4	3.75	11.43	1168	1400

Figure 33 compares the silver (Ag-110m) release fraction between the two compacts. Both PARFUME and BISON overpredict the silver release fraction by at least one-order of magnitude. After approximately 50 days, the predicted PARFUME silver release fraction is nearly identical between the two compacts. BISON predicts a higher release fraction for Compact 10-4 when compared to Compact 8-2 while the opposite is true when comparing the measured silver release fractions between the two compacts regardless of including the MDA. While the measured silver release fraction remains relatively constant during the heating tests for both compacts (i.e., Compact 8-2 at ~10^{-2}), the PARFUME and BISON release fraction increases until the end of the heating test.

Figure 34 compares the cesium (Cs-134) release fraction between the two compacts. The BISON and the measured cesium release fractions were in good agreement between the two compacts at the end of the heating test. PARFUME overpredicted the cesium release fraction by about one-order of magnitude. In general, when comparing the cesium release fractions at the same heating test temperature, the compacts were very similar, both measured and predicted. Both PARFUME and BISON predicted a higher release fraction for Compact 8-2 when in actuality, when comparing the measured cesium release fraction, Compact 10-4 had a higher release fraction than Compact 8-2.

Figure 35 compares the strontium (Sr-90) release fraction for the two compacts. Both PARFUME and BISON overpredict the strontium release fraction when compared to the measured values. The BISON prediction between the two compacts were similar, whereas the PARFUME prediction for Compact 8-2 is approximately one-order of magnitude higher than Compact 10-4 throughout the heating test. The measured and predicted strontium release fractions from both codes for Compact 8-2 were higher than their respective values for Compact 10-4 at the end of the heating test. The predicted release fraction rate after approximately 50 days from the two compacts at 1400°C was fairly consistent with the measured release fraction rate, as all four predictions and both measured values slowly increased until the end of the heating test.

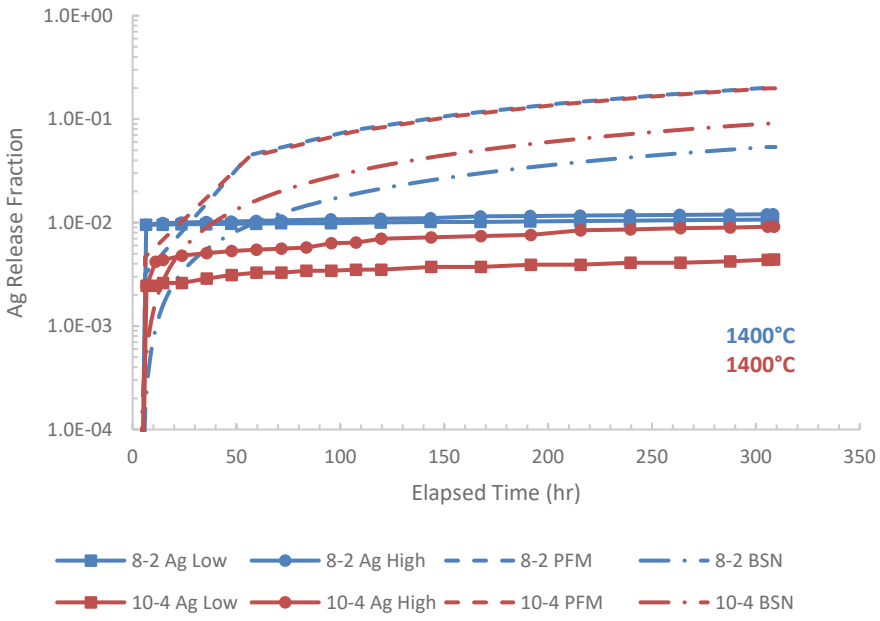

Figure 33. Measured silver (Ag-110m) release fraction versus PARFUME (PFM) and BISON (BSN) for Compacts 8-2 and 10-4 at 1400°C.

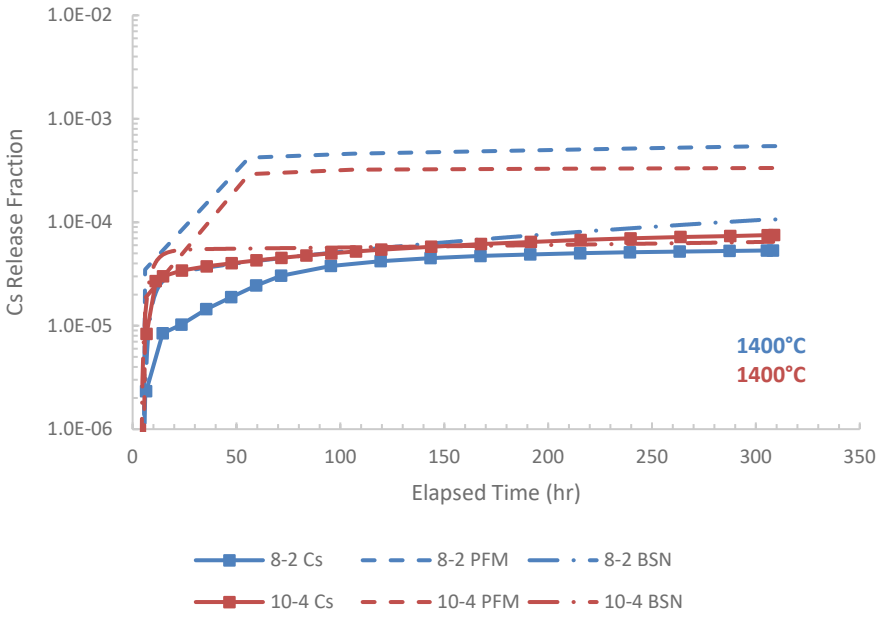

Figure 34. Measured cesium (Cs-134) release fraction versus PARFUME (PFM) and BISON (BSN) for Compacts 8-2 and 10-4 at 1400°C.

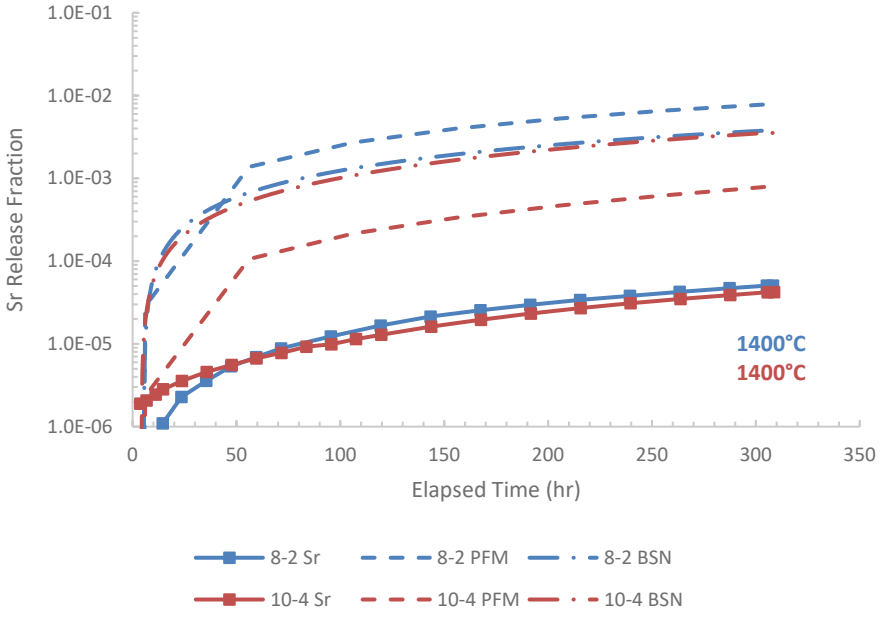

Figure 35. Measured strontium (Sr-90) release fraction versus PARFUME (PFM) and BISON (BSN) for Compacts 8-2 and 10-4 at 1400°C.

5.5 Compacts 8-2 and 10-2

Compacts 8-2 and 10-2 experienced the same TAVA temperature during the AGR-3/4 irradiation (1213°C) but were subjected to heating tests at different temperatures (1400°C and 1200°C, respectively.) Although these compacts experienced the same final TAVA temperature, the actual daily irradiation

temperatures varied as previously illustrated in Figure 10. Recall from Section 3.2 that Compact 10-2 experienced higher daily temperatures during the first half of the irradiation while Compact 8-2 was hotter near the end of the irradiation. This resulted in the compacts having different silver release fractions at the end of the irradiation, specifically 56% for Compact 8-2 and 34% for Compact 10-2. In addition, Compact 8-2 also experienced a higher fluence and burnup level resulting in more fission product inventory available to be released. The irradiations conditions for these two compacts are summarized in Table 18.

Table 18. Irradiation conditions and heating test temperature for Compacts 8-2 and 10-2.

Compact	Fluence (10^{25} n/m^2)	Burnup (%FIMA)	TAVA Irradiation Temp. (°C)	Heating Test Temp. (°C)
8-2	5.11	14.58	1213	1400
10-2	4.01	11.96	1213	1200

Figure 36 plots the measured and predicted silver release fractions during the heating tests for these two compacts. From Figure 36, both codes predicted a higher silver release fraction for Compact 8-2 when compared to Compact 10-2, which was expected since it experienced a higher heating test temperature. However, the measured silver release for compact 10-2 was higher. It is speculated that the actual silver release rate is higher over a range of intermediate temperatures (between 1100°C and 1300°C), which is supported by previous measurements from the AGR-1 heating tests (Stempien, et al. 2018). This phenomenon is not captured in the models and will therefore have to be investigated further to accurately predict silver release in this intermediate temperature range. The measured and predicted cesium release fractions (Figure 37) behaved as expected where the release fractions were higher for Compact 8-2 at the higher heating test temperature when compared to Compact 10-2. The same can be said for strontium, as illustrated in Figure 38.

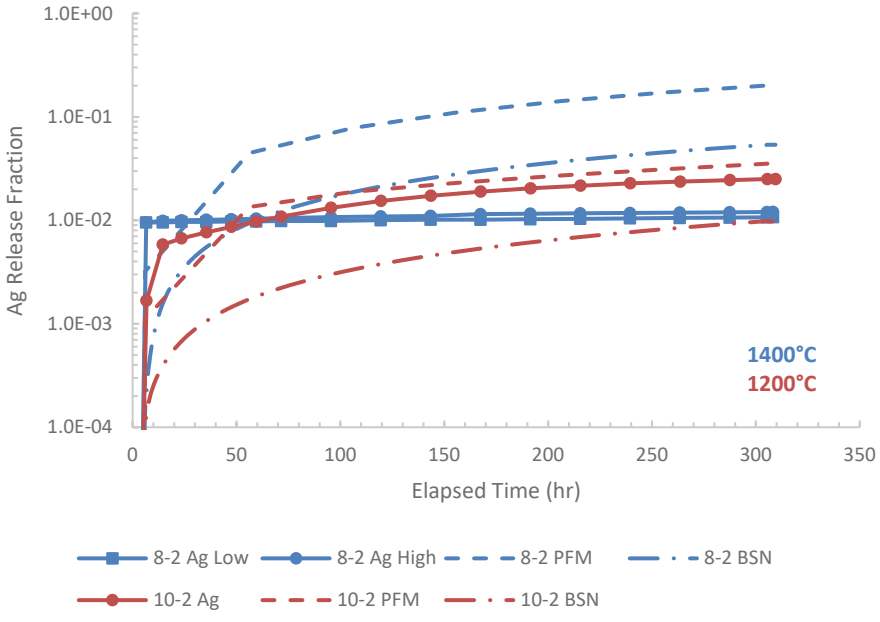

Figure 36. Measured silver (Ag-110m) release fraction versus PARFUME (PFM) and BISON (BSN) for Compacts 8-2 and 10-2.

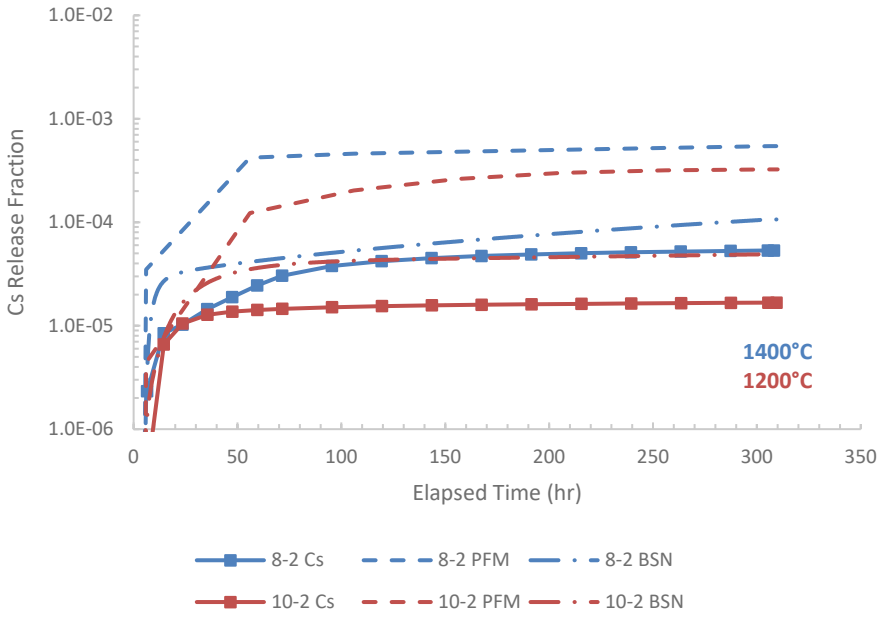

Figure 37. Measured cesium (Cs-134) release fraction versus PARFUME (PFM) and BISON (BSN) for Compacts 8-2 and 10-2.

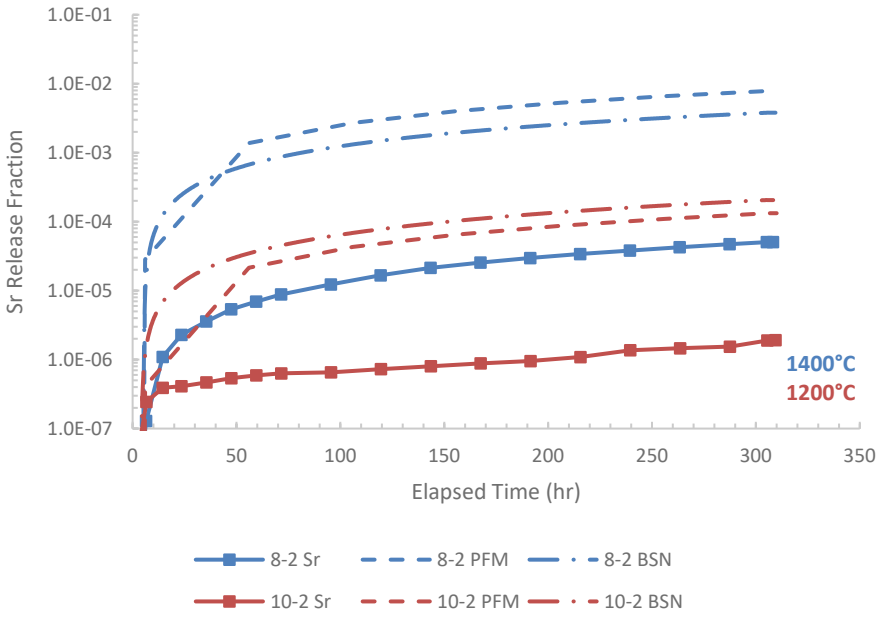

Figure 38. Measured strontium (Sr-90) release fraction versus PARFUME (PFM) and BISON (BSN) for Compacts 8-2 and 10-2.

6. CONCLUSION

PARFUME and BISON were used to predict the fission product release fraction from four AGR-3/4 as-irradiated fuel compacts during their respective heating tests. Predictions were then compared to the measured fission product release fractions collected during the heating tests in the FACS furnace at INL. These heating tests were conducted at temperatures between 1200°C and 1700°C. With the exception of silver in Compact 10-2, fission product release fractions, both measured and predicted, increased with increasing heating test temperatures consistent with previous heating test results from AGR-1 and AGR-2.

Predictions between the two models and the measured release fractions identified the following trends:

- Silver:
    - PARFUME overpredicted the silver release fractions from all four compacts and BISON overpredicted in three of the compacts (with Compact 10-2 being the exception).
    - Excluding Compact 10-2, PARFUME and BISON overpredicted the silver release during the heating tests by a factor of one to two orders of magnitude.
    - Models predict nearly all of the silver from DTF particles have been released during the irradiation and the predicted release fractions are from driver fuel particles only. The overprediction of silver therefore is a result of an overestimation of the silver diffusivities used in PARFUME and BISON for the SiC layer in the driver fuel particles.
    - The UO_2 IAEA diffusivities used in the codes for UCO might be too high, but the available data do not allow for a definitive conclusion.
    - Measurement observations from Compact 10-2 indicate Ag-110m release increases between the intermediate temperatures of 1100–1300°C which is not captured in the fuel performance models.
- Cesium
    - Both PARFUME and BISON overpredict the cesium release fraction and release fraction rate when compared to measured values leading to speculation that the cesium diffusivities used in the two codes are overestimated.
    - No additional cesium release is observed during the heating test from failed particles and no driver fuel particle failures are predicted by PARFUME. In addition, the cesium inventory from DTF particles is expected to be released during the irradiation. This would indicate that the cesium release is dominated by as-fabricated uranium contamination in the matrix amplifying the cesium release overprediction by the two codes.
    - Consistent with comparisons from the AGR-1 heating tests and model predictions, the overprediction of cesium release by the two codes from the AGR-3/4 heating tests can be partially attributed to an overestimation of the diffusivity for UCO.
- Strontium
    - The modeling codes both consistently overpredict the strontium release fraction and release fraction rates indicating the diffusivities used in PARFUME and BISON are too high.
    - The strontium inventory from DTF particles is not completely depleted during irradiation, leaving residual strontium available to be released during the heating test. This does not

allow the strontium release during the heating test to be distinguished between DTF particles and driver fuel particles.

- The overprediction of strontium can be attributed to an overestimation of the diffusivities used for UCO, SiC, compact matrix, or possibly all three.

With the exception of Compact 8-2, the measured fission product release fractions have previously been reported in a preliminary assessment of the heating tests of as-irradiated AGR-3/4 compacts (Stempien, et al. 2018). Although there is high confidence in the data presented in this report for Compact 8-2, heating test measurement results from this compact described in this report have yet to be formally published and the values presented herein should be considered preliminary.

As this report shows, validating fission product transport is difficult due to the complexities of the experiments and their associated uncertainties. AGR-3/4 heating test modeling predictions are dependent on how well the two codes account for the fission product inventories in intact particles, DTF particles, and in the compact matrix at the end of irradiation prior to performing the actual heating test predictions. There is also uncertainty in the source of fission products released during the heating tests, since only the cumulative compact release is measured, and this can complicate comparison with the models.

The overall conclusion is that both codes overpredict the release of the three fission products under consideration from the heating tests of the four as-irradiated AGR-3/4 compacts described in this report. This overestimation of fission product release by the codes can be interpreted as the fission product transport models used by PARFUME and BISON conservatively estimating the release of silver, cesium, and strontium. Further investigations are currently being conducted from the AGR experiments, including obtaining additional PIE data and performing additional heating tests, to refine and establish more accurate and appropriate fission product diffusivities used by the fuel performance models. This will allow PARFUME and BISON to estimate the transport of fission products more accurately through the UCO kernel, TRISO particle layers, and compact matrix.

7. REFERENCES

Barnes, C. M. 2006a. *AGR-1 Fuel Product Specification and Characterization Guidance.* EDF-4380, Rev. 8, Idaho National Laboratory.

Barnes, C. M. 2006b. *AGR-3 & 4 Fuel Product Specification.* EDF-6638, Rev 1, Idaho National Laboratory.

BWXT. 2006. "Industrial Fuel Fabrication and Development Lot G73V-20-69303." Data Certification Package, BWX Technologies.

CEGA. 1993. *NP-MHTGR Material Models of Pyrocarbon and Pyrolytic Silicon Carbide.* CEGA-002820, Rev. 1, CEGA Corporation.

Collin, B. P. 2016. "AGR-3/4 Irradiation Test Final As-Run Report." INL/EXT-15-35550, Rev. 1, Idaho National Laboratory.

Collin, B. P. 2014. *Comparison of Fission Product Release Predictions Using PARFUME with Results from the AGR-1 Safety Test.* INL/EXT-14-31976, Idaho National Laboratory.

Demkowicz, P. A. 2017. "AGR-3/4 Phase 2 Post-Irradiation Examination Plan." PLN-5382, Rev. 0, Idaho National Laboratory.

Demkowicz, P. A., D. V. Laug, D. M. Scates, E. L. Reber, L. G. Roybal, J. B. Walter, J. M. Harp, and R. N. Morris. 2012. "The Fuel Accident Condition Simulator (FACS) furnace system for high temperature performance testing of VHTR fuel." *Nuclear Engineering Design* 251: 164-172.

Demkowicz, P. A., E. L. Reber, D. M. Scates, L. Scott, and B. P. Collin. 2015. "First high temperature safety tests of AGR-1 TRISO fuel with the Fuel Accident Condition Simulator (FACS) furnace." *Journal of Nuclear Materials* 464: 320-330.

Hales, J. D. 2021. *BISON TRISO Modeling Advancements and Validation to AGR-1 Data.* INL/EXT-20-59368, Rev. 0, Idaho National Laboratory.

Hales, J. D., A. Toptan, W. Jiang, and B. W. Spencer. 2022. "Numerical Evaluation of AGR-2 Fission Product Release." *Journal of Nuclear Materials* 558: 153325.

Harp, J. M., J. D. Stempien, and P. A. Demkowicz. 2021. "Gamma Spectrometry Examination of the AGR-3/4 Irradiation." Idaho National Laboratory, INL/EXT-20-58254, Rev. 1.

Hawkes, G. L. 2016. "AGR-3/4 Daily As-Run Thermal Analyses." ECAR-2807, Rev. 1, Idaho National Laboratory.

Hunn, J. D. 2011. *Data Compilation for AGR-3/4 Designed-To-Fail (DTF) Fuel Particle Batch LEU03-07DTF.* ORNL/TM-2011/109, Oak Ridge National Laboratory.

Hunn, J. D. 2007. *Data Compilation for AGR-3/4 Driver Fuel Coated Particle Composite LEU03-09T.* ORN/TM-2007/019, Oak Ridge National Laboratory.

IAEA. 1997. "Fuel Performance and Fission Product Behaviour in Gas Cooled Reactors." TECDOC-9787.

Jiang, W., G. Singh, J. D. Hales, A. Toptan, B. W. Spencer, S. R. Novascone, S. L. N. Dhulipala, and Z. M. Prince. 2022. "Efficient High-fidelity TRISO Statistical Failure Analysis using BISON: Applications to AGR-2 Irradiation Testing." *Journal of Nuclear Materials* 562: 153585.

Jiang, W., J. D. Hales, B. W. Spencer, B. P. Collin, A. E. Slaughter, S. R. Novascone, A. Toptan, K. A. Gamble, and R. Gardner. 2021. "TRISO Particle Fuel Performance and Failure Analysis with BISON." *Journal of Nuclear Materials* 548: 152795.

Kovacs, W. J., K. Bongartz, and D. T. Goodin. 1985. "High-Temperture Gas-Cooled Reactor Fuel Pressure Vessel Peerformance Models." *Nuclear Technology* 68: 344-354.

Longhurst, G. R., D. F. Holland, J. L. Jones, and B. J. Merrill. 1992. "TMAP4 User's Manual." Idaho National Laboratory, EGG-FSP-10315.

Maki, J. T. 2011. *AGR-3/4 Irradiation Test Specification.* SPC-1345, Idaho National Laboratory.

Marshall, D. W. 2011. *AGR-3/4 DTF Fuel and Capsule Component Material Specifications.* SPC-1214, Rev. 1, Idaho National Laboratory.

Martin, D. G. 2002. "Considerations Pertaining to the Achievement of High Burn-ups in HTR Fuel." *Nuclear Engineering and Design* 213: 241-258.

Miller, G. K., and D. L. Knudson. 2007. "AGR-1 Pre-Test Prediction Analysis using the PARFUME Code." Idaho National Laboratory, EDF-5741, Rev. 1.

Miller, G. K., D. A. Petti, J. T. Maki, D. L. Knudon, and W. F. Skerjanc. 2023. *PARFUME Theory and Model Basis Report.* INL/EXT-08-14497, Rev. 2, Idaho National Laboratory.

Miller, G. K., D. A. Petti, J. T. Maki, D. L. Knudson, and W. F. Skerjanc. 2018. "PARFUME Theory and Model Basis Report." INL/EXT-08-14497, Rev. 1, Idaho National Laboratory.

Mitchell, T. R., and P. A. Demkowicz. 2022. *Technical Program Plan for INL Advanced Reactor Technologies Advanced Reactor Fuel Developement and Qualification Program.* PLN-3636, Rev. 11, Idaho National Laboratory.

Morris, R. N., P. A. Demkowicz, J. D. Hunn, C. A. Baldwin, and E. L. Reber. 2014. "Performance of AGR-1 High Temperature Reactor Fuel During Post-irradiatin Heating Tests." *Proceedings of the HTR 2014 Conference.* Wehai, China, October 17-31, 2014.

Ougouag, A., and C. Jiang. 2019. *CO Production Model Analysis for Correlations into PARFUME.* ECAR-4734, Rev. 0, Idaho National Laboratory.

Permann, C. J., D. R. Gaston, D. Andrs, R. W. Carlsen, F. Kong, A. D. Lindsay, J. M. Miller, et al. 2020. "MOOSE: Enabling Massively Parallel Multiphysics Simulation." *SoftwareX* 11: 100430.

Skerjanc, W. F. 2020. *Comparison of Fission Product Release Predictions using PARFUME with Results from the AGR-2 Irradation Experiment.* INL/EXT-20-59448, Rev. 0, Idaho National Laboratory.

Skerjanc, W. F., and B. P. Collin. 2018. *Assessment of Material Properties for TRISO Fuel Particles used in PARFUME.* INL/EXT-18-44631, Rev. 0, Idaho National Laboratory.

Skerjanc, W. F., and W. Jiang. 2022. *Comparison of Fission Product Release Predictions using PARFUME and BISON with Results from the AGR-3/4 Irradiation Experiment.* INL/RPT-22-69003, Rev. 0, Idaho National Laboratory.

Stempien, J. D, P. A. Demkowicz, E. L. Reber, and C. L. Christensen. 2018. "Preliminary results from the first round of post irradiation heating tests of fuel compacts from the AGR 3/4 irradiation." *Proceedings of HTR 2018.* HTR 2018-3023.

Sterbentz, J. W. 2015. "JMOCUP As-Run Daily Physics Depletion Calculation for the AGR-3/4 TRISO Particle Experiment in ATR Northeast Flux Trap." ECAR-2753, Rev. 1, Idaho National Laboratory.

Williamson, R. L., J. D. Hales, S. R. Novascone, G. Pastore, K. A. Gamble, B. W. Spencer, W. Jiang, et al. 2021. "BISON: A Flexible Code for Advanced Simulation of the Performance of Multiple Nuclear Fuel Forms." *Nuclear Technology* 207 (7): 954 - 980.